

Non-equilibrium hole dynamics in antiferromagnets: damped strings and polarons

K. Knakkegaard Nielsen,¹ T. Pohl,¹ and G. M. Bruun^{1,2}

¹*Department of Physics and Astronomy, Aarhus University, Ny Munkegade, 8000 Aarhus C, Denmark*

²*Shenzhen Institute for Quantum Science and Engineering and Department of Physics, Southern University of Science and Technology, Shenzhen 518055, China*

(Dated: March 10, 2022)

We develop a nonperturbative theory for the hole dynamics in antiferromagnetic spin lattices, as described by the t - J model. This is achieved by generalizing the self-consistent Born approximation to non-equilibrium systems, making it possible to calculate the full time-dependent many-body wave function. Our approach reveals three distinct dynamical regimes, ultimately leading to the formation of magnetic polarons. The initial hole motion is found to be ballistic but slower than a free quantum walk due to zero-point spin fluctuations. Afterwards, the coherent formation of string excitations gives rise to characteristic oscillations in the hole density. Eventually, the damping of these strings leaves behind magnetic polarons undergoing ballistic motion with a greatly reduced velocity. The developed theory provides a rigorous framework for understanding the non-equilibrium physics of defects in quantum magnets and quantitatively explains recent observations from cold-atom quantum simulations in the strong coupling regime.

Understanding the motion of charge carriers in a quantum spin environment is of great fundamental significance in condensed matter physics [1–5]. Recently, this problem is attracting growing interest [6–15], driven by the success of quantum simulations with ultracold atoms in optical lattices [16, 17] that now enable unprecedented laboratory studies. In particular, the realization of the Fermi-Hubbard model [18–34], combined with single-site resolution imaging techniques [35–38] makes it possible to probe the structure and quantum dynamics of lattice defects on a microscopic level [26, 27, 33]. The behavior of holes in the Fermi-Hubbard model and the associated formation of magnetic polarons is intimately connected to the physics of high-temperature superconductivity [39–41], and their dynamics constitutes a paradigmatic example of a strongly interacting quantum many-body system out of equilibrium, whose understanding has remained incomplete.

The rigorous description of the propagation of holes in a strongly interacting spin lattice has remained an open theoretical problem. Quantum Monte-Carlo simulations [6, 7] have allowed to study the short-time dynamics at infinite temperature and discovered a crossover from an initial free quantum walk towards a diffusive regime. Recent cold-atom experiments succeeded to trace the microscopic motion of holes in a simulated Fermi-Hubbard model [33], and instead found a transition between free ballistic hole propagation to another ballistic regime with a reduced effective hole velocity. This presents experimental indication for the creation of magnetic polarons and raises exciting open questions about the dynamical process of quasiparticle formation [42] and their emerging transport properties.

Here, we address this problem and develop a rigorous theoretical framework for the non-equilibrium dynamics of holes in an antiferromagnetic spin lattice. Our starting point is the self-consistent Born approximation

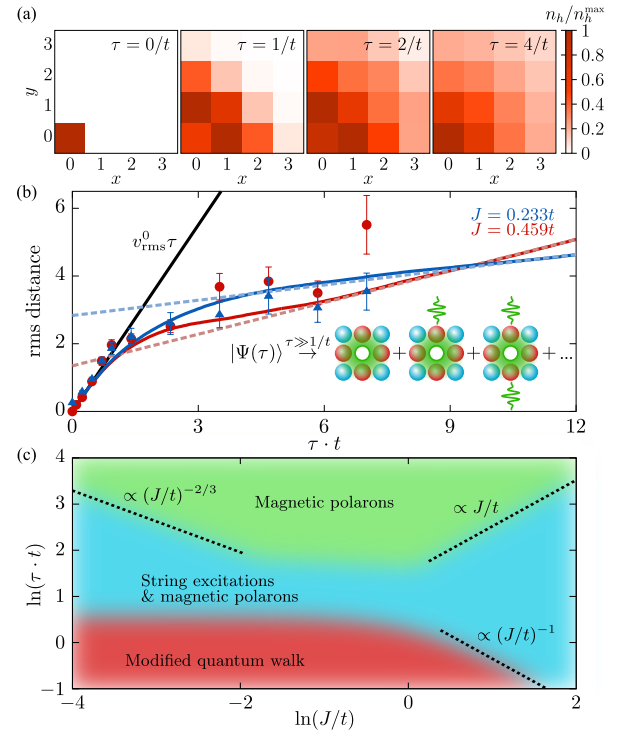


FIG. 1. Non-equilibrium hole dynamics. (a) The hole density $n_h(\mathbf{d})$ for $J = 0.233t$ and different times normalized to its maximal value n_h^{\max} is shown in the first quadrant of the lattice, exploiting the C_4 rotational symmetry. (b) Rms distance of the hole as a function of time for indicated interaction strengths compared to experimental results. At long times, the dynamics is determined by the ballistic propagation of magnetic polarons (white hole surrounded by red $\sigma = \uparrow$ and blue $\sigma = \downarrow$ fermions), dressed by a finite number of spin waves (green waves) (inset). (c) We find three distinct dynamical regimes: a modified quantum walk at short times (red region), interfering string excitations at intermediate times (blue region), and ballistic transport of magnetic polarons at long times (green region).

(SCBA), which is known to be quantitatively accurate under equilibrium conditions [15, 43, 44]. We generalize this approach to non-equilibrium situations and derive a recursion relation for the time-dependent many-body wave function of the quantum magnet. This makes it possible to describe the complex quantum dynamics of interacting spins as the hole propagates through the underlying antiferromagnetic lattice, accounting for an arbitrary number of spin excitations. Our theory provides a remarkably accurate description of the experimentally observed hole motion at all measured times and strong interactions [see Fig. 1(b)]. The calculations reveal three dynamical regimes that characterize the dynamical emergence of magnetic polarons from localized lattice defects [Fig. 1(c)]. The theory predicts a ballistic hole expansion with a universal initial velocity that is independent of the interaction strength but reduced by quantum fluctuations in the ground state of the antiferromagnetic spin lattice [red region in Fig. 1(c)]. At intermediate times (blue region), the dynamics is characterized by the formation of magnetic polaron states as well as extended string excitations, in which the hole is confined in the linear potential of flipped spins in its trail [1, 9, 45, 46]. Quantum interference between the polarons and the string excitations leads to characteristic oscillations in the hole dynamics consistent with experimental observations [33]. Ultimately, string excitations are found to dampen at long times, leading to the emergence of quasiparticle behaviour and a ballistic propagation of magnetic polarons with a reduced velocity [green region in Fig. 1(c)].

The system.— We consider the motion of a single hole in a two-component (spin $\sigma = \uparrow, \downarrow$) Fermi gas in a 2D square lattice. For strong repulsion, the two spins form a quantum antiferromagnet and the system can be described by the t - J model [41, 47, 48]. Using a so-called slave-fermion representation, this problem can be mapped to the Hamiltonian

$$\hat{H} = \sum_{\mathbf{k}} \omega_{\mathbf{k}} \hat{b}_{\mathbf{k}}^\dagger \hat{b}_{\mathbf{k}} + \sum_{\mathbf{q}, \mathbf{k}} g(\mathbf{q}, \mathbf{k}) [\hat{h}_{\mathbf{q}+\mathbf{k}}^\dagger \hat{h}_{\mathbf{q}} \hat{b}_{-\mathbf{k}}^\dagger + \text{H.c.}], \quad (1)$$

within linear spin-wave theory [2, 4, 14, 43, 44]. Here, $\hat{b}_{\mathbf{k}}^\dagger$ is a bosonic operator creating a spin wave with crystal momentum \mathbf{k} and energy $\omega_{\mathbf{k}} = 2J\sqrt{1 - \alpha^2 \gamma_{\mathbf{k}}^2}$, where $J > 0$ is the antiferromagnetic coupling between neighbouring spins and $\gamma_{\mathbf{k}} = [\cos(k_x) + \cos(k_y)]/2$ is a structure factor taking the lattice constant to be unity. We have introduced the anisotropy parameter α of the spin-spin coupling so that $\alpha = 0$ and $\alpha = 1$ corresponds to the Ising and Heisenberg limits respectively. The second term in Eq. (1) describes how the motion of holes created by the fermionic operator $\hat{h}_{\mathbf{k}}$ makes spin excitations above the antiferromagnetic ground state defined by $\hat{b}_{\mathbf{k}} |\text{AF}\rangle = 0$. The vertex strength for the scattering processes is $g(\mathbf{q}, \mathbf{k}) = 4t \cdot (u_{\mathbf{k}} \gamma_{\mathbf{q}+\mathbf{k}} - v_{\mathbf{k}} \gamma_{\mathbf{q}}) / \sqrt{N}$ with N the number of lattice sites, t the hopping

strength, and $u_{\mathbf{k}} = [(1/\sqrt{1 - \alpha^2 \gamma_{\mathbf{k}}^2} + 1)/2]^{1/2}$ and $v_{\mathbf{k}} = \text{sgn}(\gamma_{\mathbf{k}})[(1/\sqrt{1 - \alpha^2 \gamma_{\mathbf{k}}^2} - 1)/2]^{1/2}$ the coherence factors. The t - J model is an effective low energy description for strong coupling $J \ll t$ of the Hubbard model realized experimentally [41, 47, 48], and we therefore predominantly focus on this regime.

Time-dependent SCBA.— We now describe our time-dependent theory for the hole dynamics in the antiferromagnetic lattice. To describe the experimental situation, we take the initial state to be a single hole at the site $\mathbf{d} = \mathbf{0}$, i.e. $|\Psi(\tau=0)\rangle = \hat{h}_{\mathbf{0}}^\dagger |\text{AF}\rangle = \sum_{\mathbf{p}} \hat{h}_{\mathbf{p}}^\dagger |\text{AF}\rangle / \sqrt{N}$. Here, we use τ as the variable for time to distinguish it from the particle hopping t . We then have $|\Psi(\tau)\rangle = \sum_{\mathbf{p}} |\Psi_{\mathbf{p}}(\tau)\rangle / \sqrt{N}$, with $i\partial_\tau |\Psi_{\mathbf{p}}(\tau)\rangle = \hat{H} |\Psi_{\mathbf{p}}(\tau)\rangle$. We write $|\Psi_{\mathbf{p}}(\tau)\rangle = |\Psi_{\mathbf{p}}^{\text{R}}(\tau)\rangle + |\Psi_{\mathbf{p}}^{\text{A}}(\tau)\rangle$, where $|\Psi_{\mathbf{p}}^{\text{R}}(\tau)\rangle = \exp(-i\eta\tau)\theta(\tau) \cdot |\Psi_{\mathbf{p}}(\tau)\rangle$ and $|\Psi_{\mathbf{p}}^{\text{A}}(\tau)\rangle = \exp(i\eta\tau)\theta(-\tau) \cdot |\Psi_{\mathbf{p}}(\tau)\rangle$ are the retarded and advanced wave functions, respectively. Fourier transforming the Schrödinger equation then yields [49]

$$(\omega + i\eta) |\Psi_{\mathbf{p}}^{\text{R}}(\omega)\rangle = i |\Psi_{\mathbf{p}}(\tau=0)\rangle + \hat{H} |\Psi_{\mathbf{p}}^{\text{R}}(\omega)\rangle. \quad (2)$$

The advanced state is found by $|\Psi_{\mathbf{p}}^{\text{A}}(\omega)\rangle = [|\Psi_{\mathbf{p}}^{\text{R}}(\omega)\rangle]^*$. In principle, $|\Psi_{\mathbf{p}}^{\text{R}}(\omega)\rangle$ may be expanded with respect to the number of spin waves. In the strongly coupled regime, $J/t \ll 1$, however, the corresponding expansion does not truncate in a controlled way, and requires to include spin wave excitations to *infinite* order.

We resolve this problem by generalizing the self-consistent Born approximation (SCBA) [2, 4, 43, 44] to non-equilibrium conditions. Note that this approximation yields quantitatively accurate results for the hole Green's function compared to exact diagonalization on small systems [43], and Monte Carlo simulations [15]. In the spirit of the SCBA, we retain only non-crossing terms in the equations of motion for the expansion coefficients of the wave function to obtain a recursion relation for the retarded wave function (see [49] for details)

$$|\Psi_{\mathbf{p}}^{\text{R}}(\omega)\rangle = G^{\text{R}}(\mathbf{p}, \omega) [i\hat{h}_{\mathbf{p}}^\dagger |\text{AF}\rangle + \sum_{\mathbf{k}} g(\mathbf{p}, \mathbf{k}) \cdot \hat{b}_{-\mathbf{k}}^\dagger |\Psi_{\mathbf{p}+\mathbf{k}}^{\text{R}}(\omega - \omega_{\mathbf{k}})\rangle]. \quad (3)$$

Here, $G^{\text{R}}(\mathbf{p}, \omega) = [\omega - \Sigma(\mathbf{p}, \omega) + i\eta]^{-1}$ is the retarded hole Green's function with the self-energy determined by the SCBA equation [2, 4, 43, 44]

$$\Sigma(\mathbf{p}, \omega) = \sum_{\mathbf{k}} \frac{g^2(\mathbf{p}, \mathbf{k})}{\omega - \omega_{\mathbf{k}} - \Sigma(\mathbf{p}+\mathbf{k}, \omega - \omega_{\mathbf{k}}) + i\eta}. \quad (4)$$

The recursive structure evident in Eq. (3) is similar to the magnetic polaron states within the SCBA [14, 50, 51], and allows us to compute the non-equilibrium hole dynamics in an efficient and accurate manner taking an infinite number of spin wave excitations into account. This yields a rigorous generalization of the SCBA to the

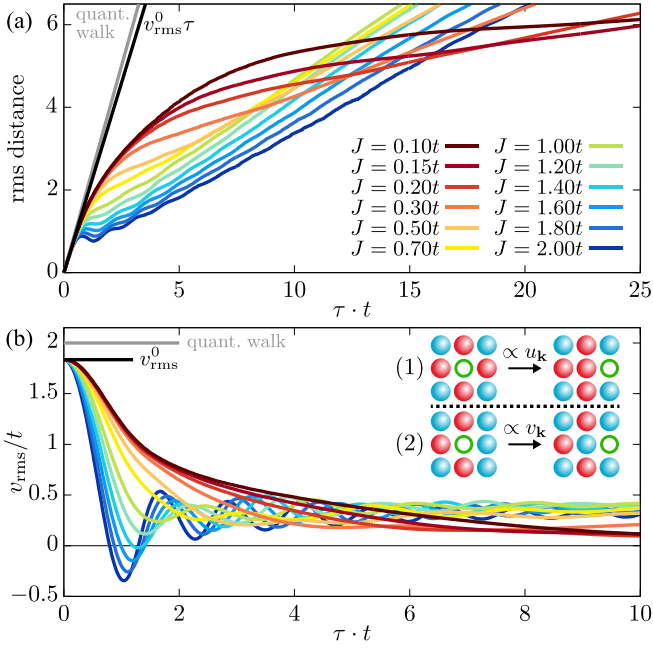


FIG. 2. **Rms distance and velocity** (a) Time evolution of the rms distance, d_{rms} , for different indicated values of $J/t = 0.1$. Panel (b) shows the rms velocity $v_{\text{rms}} = \partial_{\tau} d_{\text{rms}}$ for the same interaction strengths. The grey line corresponds to a quantum walk of a free particle with velocity $2t$ and the black line is $v_{\text{rms}}^0 \simeq 1.84t$, as obtained from Eq. (7). The inset in (b) illustrates the two pathways for the initial hole motion, whose interference leads to the observed reduction of the initial rms velocity.

time-dependent case, and represents the main result of this letter.

Using the single-site resolution of quantum gas microscopes, one can directly measure the hole density $n_h(\mathbf{d}, \tau) = \langle \Psi(\tau) | \hat{h}_{\mathbf{d}}^{\dagger} \hat{h}_{\mathbf{d}} | \Psi(\tau) \rangle$ at a given position \mathbf{d} and time τ [33]. It can be obtained from

$$n_h(\mathbf{d}, \tau) = \frac{1}{N} \sum_{\mathbf{q}} e^{-i\mathbf{q} \cdot \mathbf{d}} \int \frac{d\nu}{2\pi} N_h(\mathbf{q}, \nu), \quad (5)$$

where $N_h(\mathbf{q}, \nu) = (2\pi)^{-1} \sum_{\mathbf{p}} \int d\omega N_h(\mathbf{q}, \nu; \mathbf{p}, \omega)$ and $N_h(\mathbf{q}, \nu; \mathbf{p}, \omega) = \sum_{\mathbf{k}} \langle \Psi_{\mathbf{p}+\mathbf{q}}(\omega+\nu) | \hat{h}_{\mathbf{p}+\mathbf{q}+\mathbf{k}}^{\dagger} \hat{h}_{\mathbf{p}+\mathbf{k}} | \Psi_{\mathbf{p}}(\omega) \rangle$. Using Eq. (3), we obtain a set of self-consistency equations for $N_h(\mathbf{q}, \nu; \mathbf{p}, \omega)$ [49] and can, thereby, determine the time-dependent hole density $n_h(\mathbf{d}, \tau)$ in a non-perturbative manner.

Hole dynamics.— In Fig. 1(a), we plot the hole density in the lattice at different times for $J/t = 0.233$. This illustrates how the spatial expansion of the hole following its localized creation at site $\mathbf{d} = \mathbf{0}$. From the density we can determine the root-mean-square (rms) distance

$$d_{\text{rms}}(\tau) = \sqrt{\sum_{\mathbf{d}} d^2 \cdot n_h(\mathbf{d}, \tau)}, \quad (6)$$

which is compared to experimental measurements [33] in Fig. 1(b) for two different coupling strengths. We find a clear crossover between distinct regimes of ballistic expansion with $d = v\tau$ with different velocities v . The final expansion velocity is greatly reduced compared to a free quantum walk of the hole. For the relevant case of strong coupling, $J = 0.233t$, for which the t - J model accurately describes the underlying Fermi-Hubbard Hamiltonian, our theory agrees quantitatively with the experimental data across all timescales.

The expansion dynamics is investigated in more detail in Fig. 2, which displays the rms distance and the associated expansion velocity $v_{\text{rms}} = \partial_{\tau} d_{\text{rms}}$ for a range of interaction strengths. This shows that the crossover to the long-time ballistic motion of the polaron slows down with increasing interaction strength t/J . Physically, a hole in a lattice with a smaller spin-spin coupling, J , compared to the hopping strength, t , will move further away from its initial position before it is affected by the underlying spin order of the quantum magnet. On the other hand, however, a smaller value of J implies a stronger dressing of the hole by spin waves in its final polaron state. This slows down the long-time ballistic expansion and thereby leads to the non-trivial crossing of the lines in Fig. 2(a). The calculated dynamics reveals three distinct dynamical regimes: (i) a modified initial quantum walk of the hole, (ii) a crossover stage driven by string excitations and (iii) the final formation of magnetic polarons.

(i) *Modified quantum walk.*— The results of Figs. 1 and 2 clearly indicate a universal initial hole dynamics that follows a ballistic expansion with a J -independent velocity, v_{rms}^0 . While one may naturally expect a free quantum walk with $v_{\text{rms}}^0 = 2t$ for this initial motion [33], a closer inspection reveals that the actual velocity is slightly smaller than this value. This can be understood by expanding our non-equilibrium wave function in orders of τ and computing the short-time rms distance [49]

$$d_{\text{rms}} \simeq v_{\text{rms}}^0 \cdot \tau [1 - c_3 \cdot (t \cdot \tau)^2], \quad (7)$$

where $c_3 = c_3^{(0)} + c_3^{(J)} \cdot (J/t)^2$, and the coefficients $c_3^{(0)}$, $c_3^{(J)}$ only depend on the anisotropy parameter, α , of the spin-spin coupling [49]. Explicitly, the initial velocity is given by $v_{\text{rms}}^0 = 2f(\alpha)t$ with $f(\alpha) = [\sum_{\mathbf{k}} |u_{\mathbf{k}} e^{-i\mathbf{k} \cdot \mathbf{d}} - v_{\mathbf{k}}|^2 / N]^{1/2}$, and indeed depends exclusively on α . In the Heisenberg limit, $\alpha = 1$, we find $v_{\text{rms}}^0 \simeq 1.84t$, whereas we recover the free quantum walk value $v_{\text{rms}}^0 = 2t$ for the Ising case $\alpha = 0$. The slight slowdown for $\alpha \neq 0$ is due to the presence of zero-point spin fluctuations, which generate two ways in which the hole can make its initial move to a neighbouring site [see inset of Fig. 2(b)]: (1) it can create a spin excitation at the initial site, $d = 0$, with an amplitude $u_{\mathbf{k}}$. (2) it can absorb a spin excitation from the neighbouring site it moves to, $d = 1$, with amplitude $v_{\mathbf{k}}$. These two pathways can interfere destructively and, thereby, reduce the hopping amplitude for the ini-

tial dynamics. In the Ising limit, only the first pathway survives, such that $f(0) = 1$ and the initial hole motion recovers a free quantum walk with $v_{\text{rms}}^0 = 2t$. Setting $1 - c_3(t\tau_s)^2 = 1/2$ allows us to define the timescale τ_s , after which the initial ballistic behaviour breaks down. This yields the upper limit

$$\tau_s = \frac{1}{\sqrt{2 \left[c_3^{(0)} + c_3^{(J)} \cdot (J/t)^2 \right] t}}, \quad (8)$$

of the initial ballistic regime shown by the red area in Fig. 1(c). Consequently, we find that τ_s is independent of J/t for strong coupling $J/t \gg 1$, while it is proportional to t/J for weak coupling $J \gg t$.

(ii) *Interfering string excitations.*— After the initial universal ballistic expansion, the dynamics enters a second regime characterized by oscillations of the hole velocity with a period that increases with the interaction strength t/J . This is explored further in Fig. 3, where we show the density of holes around its initial position, $\mathbf{d} = \mathbf{0}$. Indeed, we find significant oscillations, which are consistent with the observations in the experiment [33]. The agreement between theory and experiment is particularly good at $d = 0$ [Fig. 3(a)], and $d = 1$ [Fig. 3(b)]. At larger distances, an accurate comparison becomes more difficult due to a decreasing signal-to-noise ratio in the measurements [33].

To understand the origin of the characteristic oscillations, we show the total density of states (DOS) $A(\omega) = \sum_{\mathbf{p}} A(\mathbf{p}, \omega)/N$ for $J/t = 0.233$ in Fig. 3(e), and as a function of J/t in Fig. 3(f). Here, $A(\mathbf{p}, \omega)$ is the hole spectral function [49]. One clearly observes multiple peaks in the DOS, the lowest of which originates from the emerging magnetic polaron. On the other hand, Fig. 3(e) reveals a characteristic $(J/t)^{2/3}$ -scaling of the position of the high-frequency peaks, revealing the existence of string excitations. These correspond to Airy-like eigenstates of the hole, confined in the linear potential formed by its trail of flipped spins. In the strong coupling limit of the t - J_z model, this effective potential has a strength $\propto J_z$ [1, 4, 9, 45, 46]. The presence of transverse spin-spin couplings broadens the string excitations [15, 46], and we find that their spectral widths show the same $(J/t)^{2/3}$ scaling behaviour as their energies.

In order to analyze further how these excitations contribute to the intermediate hole dynamics, we use a multi-Lorentzian fit to the spectral function as shown by the dashed line in Fig. 3(e). Its Fourier transform, $\hat{A}(\tau)$, exclusively captures the contribution from the different peaks and the norm square, $|\hat{A}(\tau)|^2$, recovers the oscillatory hole motion as shown in the inset of Fig. 3(a). Indeed, it follows from Eq. (3) that $|\hat{A}(\tau)|^2$ determines the hole density at the initial site $\mathbf{d} = \mathbf{0}$ to the lowest order in the number of spin waves. We can, thus, conclude from Fig. 3(a) that the oscillations of $n_h(d = 0, \tau)$ are a

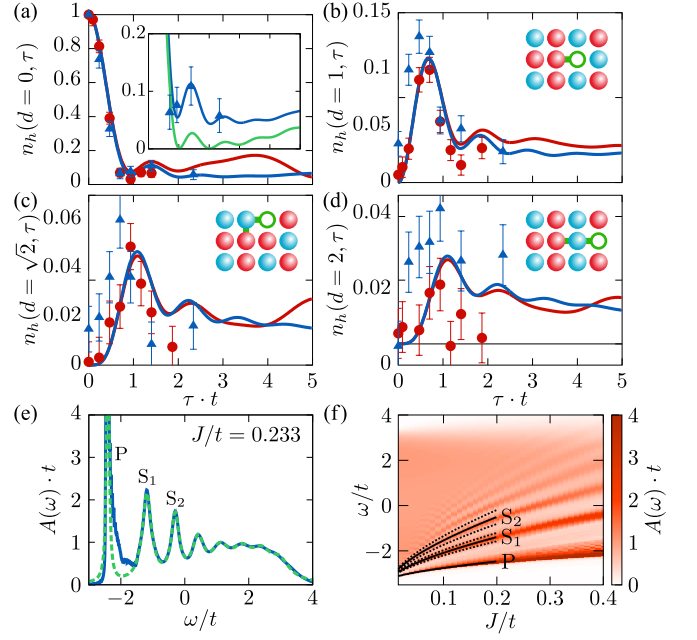


FIG. 3. **Local hole density and string excitations.** The hole density as a function of time for $J/t = 0.459$ (red) and $J/t = 0.233$ (blue), and for different indicated distances, d , from the initial site: (a) $d = 0$, (b) $d = 1$, (c) $d = \sqrt{2}$, and (d) $d = 2$. The experimental data is shown by red circles for $J/t = 0.459$ and by blue triangles for $J/t = 0.233$. (e) The total density of states $A(\omega)$ with a multi-Lorentzian fit (dashed green line). In the inset of panel (a), the norm square of the Fourier transform of this fit (green line) is compared to the full solution and experimental data (blue) for $J/t = 0.233$. The low-frequency peak of $A(\omega)$ corresponds to the magnetic polaron (marked as P), and the other peaks at higher frequencies reflect string excitations (marked as S_i). Their energies and spectral widths exhibit a characteristic $(J/t)^{2/3}$ scaling for $J/t \ll 1$, which is indicated by the black lines in panel (f).

consequence of quantum interference between the magnetic polaron states and the string excitations. In the strongly interacting regime of $J \ll t$, these oscillations extend towards longer timescales as the spacing between the associated energies decreases [see Fig. 3(f)]. This process defines the second dynamical regime that corresponds to the blue region in Fig. 1(c), while the lifetime of the lowest string excitation [marked as S_1 in Fig. 3(f)] determines the dynamical crossover into the final propagation stage. The corresponding transition time scales as $(J/t)^{-2/3}$ and J/t for strong and weak coupling, respectively, and is shown by the upper dotted lines in Fig. 1(c).

(iii) *Magnetic polarons.*— Following the damping of string excitations, the remaining superposition of magnetic polaron states, once more, undergoes a ballistic expansion, but with a greatly reduced effective velocity compared to the initial hole expansion. This final ballistic expansion stage is evident from Figs. 1(b) and 2.

Indeed, at times longer than the string excitation lifetime, we can write our wave function as [49]

$$|\Psi(\tau)\rangle \rightarrow \sum_{\mathbf{p}} \left[\sqrt{Z_{\mathbf{p}}} e^{-i\varepsilon_{\mathbf{p}}\tau} |\Psi_{\mathbf{p}}^{\text{pol}}\rangle + \sum_{\mathbf{k}} g_1(\mathbf{p}, \mathbf{k}) \sqrt{Z_{\mathbf{p}+\mathbf{k}}} e^{-i(\varepsilon_{\mathbf{p}+\mathbf{k}} + \omega_{\mathbf{k}})\tau} \hat{b}_{-\mathbf{k}}^\dagger |\Psi_{\mathbf{p}+\mathbf{k}}^{\text{pol}}\rangle + \dots \right], \quad (9)$$

where $g_1(\mathbf{p}, \mathbf{k}) = g(\mathbf{p}, \mathbf{k}) \text{Re}[G^{\text{R}}(\mathbf{p}, \varepsilon_{\mathbf{p}+\mathbf{k}} + \omega_{\mathbf{k}})]$. The first term in Eq. (9) corresponds to the ballistic propagation of magnetic polarons $|\Psi_{\mathbf{p}}^{\text{pol}}\rangle$ with crystal momentum \mathbf{p} , energy $\varepsilon_{\mathbf{p}}$, and quasiparticle residue $Z_{\mathbf{p}}$. The second term describes the polaron propagation with a spin wave, and is the first term in a series in the number of spin-wave excitations, as illustrated in the inset of Fig. 1(b). This asymptotic form of the many-body wave function explicitly confirms the dynamical formation of magnetic polarons, indicated by the experiments of Ref. [33].

In Fig. 4, we show the calculated asymptotic expansion velocity v_{rms}^∞ . Motivated by the propagation of magnetic polarons evident from Eq. (9), we also determine the average polaron group velocity $v_{\text{rms}}^{\text{pol}} = [\sum_{\mathbf{p}} (\nabla_{\mathbf{p}} \varepsilon_{\mathbf{p}})^2 / N]^{1/2}$. In the perturbative limit, the first term in Eq. (9) dominates, and v_{rms}^∞ and $v_{\text{rms}}^{\text{pol}}$ both approach an asymptotic value of $0.41w_{\text{pol}}$ [49]. While this agreement is confirmed in Fig. 4, the two velocities start to deviate significantly below $J/t \sim 0.4$. This is due to a qualitative change in the behavior of the quasiparticle residue, which becomes very small in certain regions of the Brillouin zone for strong interactions [49]. As a result, the associated polaron states do not contribute to the long-time dynamics, leading to the reduction in the expansion velocity seen in Fig. 4. This is consistent with the asymptotic limit of infinitely strong interactions, $J/t \rightarrow 0^+$, in which the quasiparticle residue vanishes throughout the Brillouin zone. This signals a breakdown of the quasiparticle description, yields a vanishing asymptotic expansion velocity, and indicates diffusive long-time behavior in this limit.

Conclusions. – We have developed a non-perturbative approach for computing the non-equilibrium dynamics of hole defects in doped Heisenberg antiferromagnets. Our theory provides a quantitative explanation of recent experimental results from cold-atom quantum simulations [33] at strong interactions. The method yields a complete characterization of the quantum motion of holes and reveals three distinct dynamical regimes that characterize the emergence and evolution of magnetic polarons. It explains observed oscillatory behavior in terms of quantum interference between polarons and magnetic string excitations. The presented formalism offers a powerful framework to describe the non-equilibrium quantum dynamics of impurities in strongly interacting lattice models. For example, the method could be used to analyze spectroscopic measurements [52] of holes, which may permit to probe and explore the quasiparticle properties of magnetic polarons in unprecedented detail.

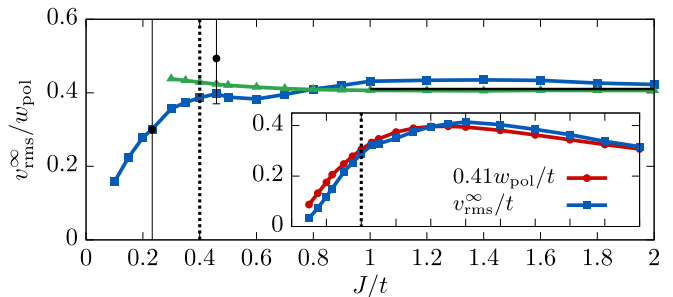


FIG. 4. **Asymptotic expansion velocity.** Long-time expansion velocity v_{rms}^∞ (blue squares) and average polaronic group velocity $v_{\text{rms}}^{\text{pol}}$ (green triangles) as a function of the inverse interaction strength, J/t , in units of the polaron energy bandwidth $w_{\text{pol}} = \varepsilon_{p=0} - \varepsilon_{p=(\pi/2, \pi/2)}$. The experimentally observed velocities are shown by the black dots. The inset compares v_{rms}^∞ and $0.41w_{\text{pol}}$ in the same range of interaction strengths J/t , and reveals a maximum in the expansion velocity around $J = t$. For $J < 0.4t$ (marked by the vertical dashed line), v_{rms}^∞ is no longer determined by the bandwidth alone.

Moreover, our approach may also be utilized to describe the dynamical build-up of correlations between two holes, providing new insights into pairing and a potential mechanism for high-temperature superconductivity at low doping [40, 48, 53–56].

The authors thank Martin Lebrat, Muqing Xu, Lev Kendrick, Anant Kale and Markus Greiner for sharing experimental data and comments on the manuscript. We appreciate helpful discussions with Jens Havgaard Nyhøgn. This work has been supported by the Danish National Research Foundation through the Center of Excellence “CCQ” (Grant agreement no.: DNRFF156).

-
- [1] W. F. Brinkman and T. M. Rice, Phys. Rev. B **2**, 1324 (1970).
 - [2] S. Schmitt-Rink, C. M. Varma, and A. E. Ruckenstein, Phys. Rev. Lett. **60**, 2793 (1988).
 - [3] B. I. Shraiman and E. D. Siggia, Phys. Rev. Lett. **61**, 467 (1988).
 - [4] C. L. Kane, P. A. Lee, and N. Read, Phys. Rev. B **39**, 6880 (1989).
 - [5] S. A. Trugman, Phys. Rev. B **41**, 892 (1990).
 - [6] J. Carlström, N. Prokof'ev, and B. Svistunov, Phys. Rev. Lett. **116**, 247202 (2016).
 - [7] M. Kánász-Nagy, I. Lovas, F. Grusdt, D. Greif, M. Greiner, and E. A. Demler, Phys. Rev. B **96**, 014303 (2017).
 - [8] F. Grusdt, Z. Zhu, T. Shi, and E. Demler, SciPost Phys. **5**, 57 (2018).
 - [9] F. Grusdt, M. Kánász-Nagy, A. Bohrdt, C. S. Chiu, G. Ji, M. Greiner, D. Greif, and E. Demler, Phys. Rev. X **8**, 011046 (2018).

- [10] F. Grusdt, A. Bohrdt, and E. Demler, *Phys. Rev. B* **99**, 224422 (2019).
- [11] A. Bohrdt, C. S. Chiu, G. Ji, M. Xu, D. Greif, M. Greiner, E. Demler, F. Grusdt, and M. Knap, *Nature Physics* **15**, 921 (2019).
- [12] A. Bohrdt, Y. Wang, J. Koepsell, M. Kánasz-Nagy, E. Demler, and F. Grusdt, *Phys. Rev. Lett.* **126**, 026401 (2021).
- [13] D. Soriano and M. I. Katsnelson, *Phys. Rev. B* **101**, 041402(R) (2020).
- [14] K. K. Nielsen, M. A. Bastarrachea-Magnani, T. Pohl, and G. M. Bruun, *Phys. Rev. B* **104**, 155136 (2021).
- [15] N. Diamantis and E. Manousakis, *New Journal of Physics* (2021).
- [16] T. Esslinger, *Annual Review of Condensed Matter Physics* **1**, 129 (2010).
- [17] C. Gross and I. Bloch, *Science* **357**, 995 (2017).
- [18] T. Esslinger, *Annual Review of Condensed Matter Physics* **1**, 129 (2010).
- [19] M. Boll, T. A. Hilker, G. Salomon, A. Omran, J. Nespolo, L. Pollet, I. Bloch, and C. Gross, *Science* **353**, 1257 (2016).
- [20] L. W. Cheuk, M. A. Nichols, K. R. Lawrence, M. Okan, H. Zhang, E. Khatami, N. Trivedi, T. Paiva, M. Rigol, and M. W. Zwierlein, *Science* **353**, 1260 (2016).
- [21] A. Mazurenko, C. S. Chiu, G. Ji, M. F. Parsons, M. Kánasz-Nagy, R. Schmidt, F. Grusdt, E. Demler, D. Greif, and M. Greiner, *Nature* **545**, 462 (2017).
- [22] T. A. Hilker, G. Salomon, F. Grusdt, A. Omran, M. Boll, E. Demler, I. Bloch, and C. Gross, *Science* **357**, 484 (2017).
- [23] P. T. Brown, D. Mitra, E. Guardado-Sanchez, P. Schauß, S. S. Kondov, E. Khatami, T. Paiva, N. Trivedi, D. A. Huse, and W. S. Bakr, *Science* **357**, 1385 (2017).
- [24] C. S. Chiu, G. Ji, A. Mazurenko, D. Greif, and M. Greiner, *Phys. Rev. Lett.* **120**, 243201 (2018).
- [25] P. T. Brown, D. Mitra, E. Guardado-Sanchez, R. Nourafkan, A. Reymbaut, C.-D. Hébert, S. Bergeron, A.-M. S. Tremblay, J. Kokalj, D. A. Huse, P. Schauß, and W. S. Bakr, *Science* **363**, 379 (2019).
- [26] J. Koepsell, J. Vijayan, P. Sompet, F. Grusdt, T. A. Hilker, E. Demler, G. Salomon, I. Bloch, and C. Gross, *Nature* **572**, 358 (2019).
- [27] C. S. Chiu, G. Ji, A. Bohrdt, M. Xu, M. Knap, E. Demler, F. Grusdt, M. Greiner, and D. Greif, *Science* **365**, 251 (2019).
- [28] P. T. Brown, E. Guardado-Sanchez, B. M. Spar, E. W. Huang, T. P. Devereaux, and W. S. Bakr, *Nature Physics* **16**, 26 (2020).
- [29] J. Vijayan, P. Sompet, G. Salomon, J. Koepsell, S. Hirthe, A. Bohrdt, F. Grusdt, I. Bloch, and C. Gross, *Science* **367**, 186 (2020).
- [30] T. Hartke, B. Oreg, N. Jia, and M. Zwierlein, *Phys. Rev. Lett.* **125**, 113601 (2020).
- [31] E. Guardado-Sanchez, A. Morningstar, B. M. Spar, P. T. Brown, D. A. Huse, and W. S. Bakr, *Phys. Rev. X* **10**, 011042 (2020).
- [32] J. Koepsell, D. Bourgund, P. Sompet, S. Hirthe, A. Bohrdt, Y. Wang, F. Grusdt, E. Demler, G. Salomon, C. Gross, and I. Bloch, *Science* **374**, 82 (2021), <https://www.science.org/doi/pdf/10.1126/science.abe7165>.
- [33] G. Ji, M. Xu, L. H. Kendrick, C. S. Chiu, J. C. Brüggengjürgen, D. Greif, A. Bohrdt, F. Grusdt, E. Demler, M. Lebrat, and M. Greiner, *Phys. Rev. X* **11**, 021022 (2021).
- [34] M. Gall, N. Wurz, J. Samland, C. F. Chan, and M. Köhl, *Nature* **589**, 40 (2021).
- [35] W. S. Bakr, J. I. Gillen, A. Peng, S. Fölling, and M. Greiner, *Nature* **462**, 74 (2009).
- [36] J. F. Sherson, C. Weitenberg, M. Endres, M. Cheneau, I. Bloch, and S. Kuhr, *Nature* **467**, 68 (2010).
- [37] E. Haller, J. Hudson, A. Kelly, D. A. Cotta, B. Peaudecerf, G. D. Bruce, and S. Kuhr, *Nature Physics* **11**, 738 (2015).
- [38] J. Yang, L. Liu, J. Mongkolkiattichai, and P. Schauss, *PRX Quantum* **2**, 020344 (2021).
- [39] V. J. Emery, *Phys. Rev. Lett.* **58**, 2794 (1987).
- [40] J. R. Schrieffer, X.-G. Wen, and S.-C. Zhang, *Phys. Rev. Lett.* **60**, 944 (1988).
- [41] E. Dagotto, *Rev. Mod. Phys.* **66**, 763 (1994).
- [42] A. Bohrdt, F. Grusdt, and M. Knap, *New Journal of Physics* **22**, 123023 (2020).
- [43] G. Martinez and P. Horsch, *Phys. Rev. B* **44**, 317 (1991).
- [44] Z. Liu and E. Manousakis, *Phys. Rev. B* **44**, 2414 (1991).
- [45] L. Bulaevskii, E. Nagaev, and D. Khomskii, *JETP* **27**, 836 (1968).
- [46] Z. Liu and E. Manousakis, *Phys. Rev. B* **45**, 2425 (1992).
- [47] K. A. Chao, J. Spalek, and A. M. Oles, *Journal of Physics C: Solid State Physics* **10**, L271 (1977).
- [48] Y. A. Izyumov, *Physics-Uspekhi* **40**, 445 (1997).
- [49] See Supplemental Material online for additional details.
- [50] G. F. Reiter, *Phys. Rev. B* **49**, 1536 (1994).
- [51] A. Ramšak and P. Horsch, *Phys. Rev. B* **57**, 4308 (1998).
- [52] A. Bohrdt, D. Greif, E. Demler, M. Knap, and F. Grusdt, *Phys. Rev. B* **97**, 125117 (2018).
- [53] B. I. Shraiman and E. D. Siggia, *Phys. Rev. B* **40**, 9162 (1989).
- [54] D. M. Frenkel and W. Hanke, *Phys. Rev. B* **42**, 6711 (1990).
- [55] R. Eder, *Phys. Rev. B* **45**, 319 (1992).
- [56] J. Riera and E. Dagotto, *Phys. Rev. B* **57**, 8609 (1998).

Supplemental Material

Non-equilibrium hole dynamics in antiferromagnets: damped strings and polarons

CONTENTS

Non-equilibrium wave function	1
Hole density dynamics	3
Short-time dynamics	3
Asymptotic polaron dynamics	7
Perturbative limit	8
Energy and lifetime of lowest string excitation	9
References	10

NON-EQUILIBRIUM WAVE FUNCTION

In this section, we generalize the self-consistent Born approximation to derive the full non-equilibrium dynamics of the state initialized as a single hole in the crystal momentum state \mathbf{p}

$$|\Psi_{\mathbf{p}}(\tau = 0)\rangle = \hat{h}_{\mathbf{p}}^{\dagger} |\text{AF}\rangle. \quad (\text{S1})$$

We use τ as time variable to distinguish it from the hopping amplitude t . It is beneficial to split the state into a retarded and advanced part, according to

$$|\Psi_{\mathbf{p}}(\tau)\rangle = |\Psi_{\mathbf{p}}^{\text{R}}(\tau)\rangle + |\Psi_{\mathbf{p}}^{\text{A}}(\tau)\rangle = e^{-\eta|\tau|} (\theta(\tau) |\Psi_{\mathbf{p}}(\tau)\rangle + \theta(-\tau) |\Psi_{\mathbf{p}}(\tau)\rangle), \quad (\text{S2})$$

in which $\eta > 0$ is a positive infinitesimal that regularizes the Fourier transformation to frequency space. The resulting equation for the retarded wave function in frequency space is, hereby,

$$(\omega + i\eta) |\Psi_{\mathbf{p}}^{\text{R}}(\omega)\rangle = i |\Psi_{\mathbf{p}}(\tau = 0)\rangle + \hat{H} |\Psi_{\mathbf{p}}^{\text{R}}(\omega)\rangle, \quad (\text{S3})$$

with $|\Psi_{\mathbf{p}}^{\text{R}}(\omega)\rangle = \int d\tau e^{+i\omega\tau} |\Psi_{\mathbf{p}}^{\text{R}}(\tau)\rangle$. The equation for $|\Psi_{\mathbf{p}}^{\text{A}}(\omega)\rangle$ can be obtained by complex conjugation. As the hole scatters and emits spin waves, the wave function can be expanded in increasing orders of spin waves,

$$|\Psi_{\mathbf{p}}^{\text{R}}(\omega)\rangle = R^{(0)}(\mathbf{p}; \omega) \cdot \hat{h}_{\mathbf{p}}^{\dagger} |\text{AF}\rangle + \sum_{\mathbf{k}} R^{(1)}(\mathbf{p}, \mathbf{k}; \omega) \cdot \hat{h}_{\mathbf{p}+\mathbf{k}}^{\dagger} \hat{b}_{-\mathbf{k}}^{\dagger} |\text{AF}\rangle + \dots \quad (\text{S4})$$

The central approximation of our work is to use the framework of the self-consistent Born approximation (SCBA). Here, only spin waves absorbed in the same order as they are emitted are taken into account. This is the exact same methodology used in [1] to establish a wave function consistent with the SCBA, which we used in our previous paper on the spatial structure of magnetic polarons [2]. From Eq. (S3), the equations of motion, thereby, become

$$\begin{aligned}
 & [\omega + i\eta] R^{(0)}(\mathbf{p}; \omega) = i + \sum_{\mathbf{k}} g(\mathbf{p}, \mathbf{k}_1) R^{(1)}(\mathbf{p}, \mathbf{k}_1; \omega), \\
 & \left[\omega + i\eta - \sum_{j=1}^n \omega_{\mathbf{k}_j} \right] R^{(n)}(\mathbf{p}, \{\mathbf{k}_j\}_{j=1}^n; \omega) = g(\mathbf{K}_{n-1}, \mathbf{k}_n) R^{(n-1)}(\mathbf{p}, \{\mathbf{k}_j\}_{j=1}^{n-1}; \omega) + \sum_{\mathbf{k}_{n+1}} g(\mathbf{K}_n, \mathbf{k}_{n+1}) R^{(n+1)}(\mathbf{p}, \{\mathbf{k}_j\}_{j=1}^{n+1}; \omega).
 \end{aligned} \quad (\text{S5})$$

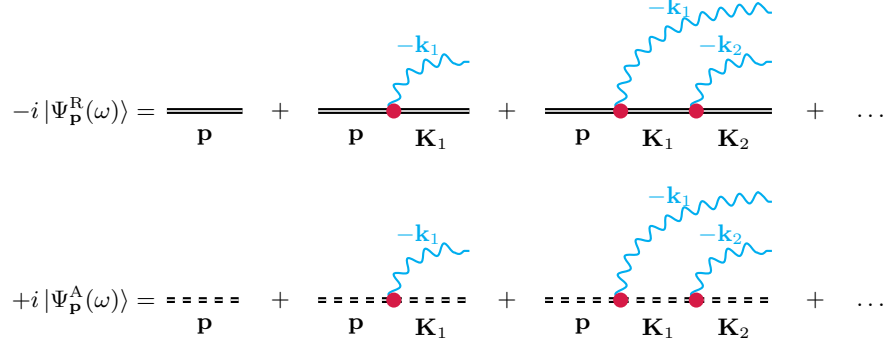


FIG. S1. Diagrammatic representation of non-equilibrium wave functions in frequency space. Green's functions labelled with \mathbf{K}_n has a shifted frequency of: $\omega - \sum_{j=1}^n \omega_{\mathbf{k}_j}$.

Inspired by the result in [1], we propose a similar recursion relation for the coefficients

$$R^{(n+1)}(\mathbf{p}, \{\mathbf{k}_j\}_{j=1}^{n+1}; \omega) = g(\mathbf{K}_n, \mathbf{k}_{n+1}) \cdot G^R(\mathbf{K}_{n+1}, \omega - \sum_{j=1}^{n+1} \omega_{\mathbf{k}_j}) \cdot R^{(n)}(\mathbf{p}, \{\mathbf{k}_j\}_{j=1}^n; \omega), \quad (\text{S6})$$

where $\mathbf{K}_n = \mathbf{p} + \sum_{j=1}^n \mathbf{k}_j$, and $\mathbf{K}_0 = \mathbf{p}$. This entails the retarded hole Green's function $G^R(\mathbf{p}, \omega) = (\omega - \Sigma(\mathbf{p}, \omega) + i\eta)^{-1}$. The self-energy is determined by the self-consistency equation inherent to the SCBA [3–6]

$$\Sigma(\mathbf{p}, \omega) = \sum_{\mathbf{k}} \frac{g^2(\mathbf{p}, \mathbf{k})}{\omega - \omega_{\mathbf{k}} - \Sigma(\mathbf{p} + \mathbf{k}, \omega - \omega_{\mathbf{k}}) + i\eta}. \quad (\text{S7})$$

Using this recursion relation at order $n + 1$ in Eq. (S5), yields

$$\left[\omega + i\eta - \sum_{j=1}^n \omega_{\mathbf{k}_j} - \Sigma \left(\mathbf{K}_n, \omega - \sum_{j=1}^n \omega_{\mathbf{k}_j} \right) \right] R^{(n)}(\mathbf{p}, \{\mathbf{k}_j\}_{j=1}^n; \omega) = g(\mathbf{K}_{n-1}, \mathbf{k}_n) R^{(n-1)}(\mathbf{p}, \{\mathbf{k}_j\}_{j=1}^{n-1}; \omega), \quad (\text{S8})$$

which by rearrangement shows the recursion relation in Eq. (S6) for order n . Finally, using this relation at order 1 yields $R^{(0)}(\mathbf{p}; \omega) = iG^R(\mathbf{p}, \omega)$. In this manner, the SCBA makes it possible to write down a wave function that takes an infinite number of spin waves into account. The explicit form of the coefficients for $n \geq 1$ is

$$A^{(n)*}(\mathbf{p}, \{\mathbf{k}_j\}_{j=1}^n; \omega) = R^{(n)}(\mathbf{p}, \{\mathbf{k}_j\}_{j=1}^n; \omega) = +iG^R(\mathbf{p}, \omega) \cdot \prod_{j=1}^n g(\mathbf{K}_{j-1}, \mathbf{k}_j) G^R(\mathbf{K}_j, \omega - \sum_{l=1}^j \omega_{\mathbf{k}_l}), \quad (\text{S9})$$

where $A^{(n)}$ are the coefficients of $|\Psi_{\mathbf{p}}^A(\omega)\rangle$. In this way, we can also write a recursive equation for the states

$$[|\Psi_{\mathbf{p}}^A(\omega)\rangle]^* = |\Psi_{\mathbf{p}}^R(\omega)\rangle = G^R(\mathbf{p}, \omega) \left[+i\hat{h}_{\mathbf{p}}^\dagger |\text{AF}\rangle + \sum_{\mathbf{k}} g(\mathbf{p}, \mathbf{k}) \cdot \hat{b}_{-\mathbf{k}}^\dagger |\Psi_{\mathbf{p}+\mathbf{k}}^R(\omega - \omega_{\mathbf{k}})\rangle \right]. \quad (\text{S10})$$

This recursive structure makes it possible for us to compute the motion of the hole with a high accuracy. It also allows us to formulate a diagrammatic expression for the wave functions as shown in Fig. S1, and corresponds to an extension of the method used in Ref. [7] for the magnetic polaron states. The diagrammatic rules are:

- (1) nth full double line: retarded hole Green's function, $G^R(\mathbf{K}_n, \varepsilon_{\mathbf{p}} - \sum_{i=1}^n \omega_{\mathbf{k}_i})$.
- (2) nth dashed double line: advanced hole Green's function, $G^A(\mathbf{K}_n, \varepsilon_{\mathbf{p}} - \sum_{i=1}^n \omega_{\mathbf{k}_i})$.
- (3) wavy blue line with momentum $-\mathbf{k}_i$: spinwave operator $\hat{b}_{-\mathbf{k}_i}^\dagger$.
- (4) nth red dot in a given diagram: interaction vertex, $g(\mathbf{K}_n, \mathbf{k}_{n+1})/\sqrt{N}$.
- (5) nth open-ended double line: hole operator, $h_{\mathbf{K}_n}^\dagger$.
- (6) finally, sum over all spinwave momenta, \mathbf{k}_i .

HOLE DENSITY DYNAMICS

In this section, we will use the dynamical crystal momentum states in the previous section to calculate the hole density dynamics. Hence, consider the density of holes

$$n_h(\mathbf{r}, \tau) = \langle \Psi(\tau) | \hat{h}_{\mathbf{r}}^\dagger \hat{h}_{\mathbf{r}} | \Psi(\tau) \rangle. \quad (\text{S11})$$

Here, the wave function $|\Psi(\tau)\rangle$ is initially given by a hole localized at the central site $|\Psi(\tau)\rangle = \hat{h}_{\mathbf{d}=0}^\dagger |\text{AF}\rangle = \frac{1}{\sqrt{N}} \sum_{\mathbf{p}} \hat{h}_{\mathbf{p}}^\dagger |\text{AF}\rangle$. By decomposing into crystal momentum and frequency components, we can, hereby, write

$$n_h(\mathbf{d}, \tau) = \frac{1}{N} \sum_{\mathbf{q}} e^{-i\mathbf{q} \cdot \mathbf{d}} N_h(\mathbf{q}, \tau), \quad (\text{S12})$$

with $N_h(\mathbf{q}, \tau) = (2\pi)^{-2} \int d\nu e^{i\nu\tau} \int d\omega \sum_{\mathbf{p}} N_h(\mathbf{q}, \nu; \mathbf{p}, \omega) / N$, and

$$N_h(\mathbf{q}, \nu; \mathbf{p}, \omega) = \sum_{\mathbf{k}} \langle \Psi_{\mathbf{p}+\mathbf{q}}(\omega + \nu) | \hat{h}_{\mathbf{p}+\mathbf{q}+\mathbf{k}}^\dagger \hat{h}_{\mathbf{p}+\mathbf{k}} | \Psi_{\mathbf{p}}(\omega) \rangle. \quad (\text{S13})$$

Furthermore, the splitting into the retarded and advanced state, $|\Psi(\omega)\rangle = |\Psi^R(\omega)\rangle + |\Psi^A(\omega)\rangle$, means that we can write

$$N_h(\mathbf{q}, \nu; \mathbf{p}, \omega) = 2\text{Re}[N_h^{\text{RR}}(\mathbf{q}, \nu; \mathbf{p}, \omega) + N_h^{\text{RA}}(\mathbf{q}, \nu; \mathbf{p}, \omega)], \quad (\text{S14})$$

with $N_h^{\text{IL}}(\mathbf{q}, \nu; \mathbf{p}, \omega) = \sum_{\mathbf{k}} \langle \Psi_{\mathbf{p}+\mathbf{q}}^{\text{I}}(\omega + \nu) | \hat{h}_{\mathbf{p}+\mathbf{q}+\mathbf{k}}^\dagger \hat{h}_{\mathbf{p}+\mathbf{k}} | \Psi_{\mathbf{p}}^{\text{L}}(\omega) \rangle$, and I, L = R, A. Using the recursive expressions in Eq. (S10), we then get

$$\begin{aligned} N_h^{\text{RR}}(\mathbf{q}, \nu; \mathbf{p}, \omega) &= G^{\text{R}*}(\mathbf{p} + \mathbf{q}, \omega + \nu) G^{\text{R}}(\mathbf{p}, \omega) \\ &\cdot \left[1 + \sum_{\mathbf{k}_1, \mathbf{k}_2} g(\mathbf{p} + \mathbf{q}, \mathbf{k}_1) g(\mathbf{p}, \mathbf{k}_2) \langle \Psi_{\mathbf{p}+\mathbf{q}+\mathbf{k}_1}^{\text{R}}(\omega + \nu - \omega_{\mathbf{k}_1}) | \hat{b}_{-\mathbf{k}_1} \sum_{\mathbf{k}_3} \hat{h}_{\mathbf{p}+\mathbf{q}+\mathbf{k}_3}^\dagger \hat{h}_{\mathbf{p}+\mathbf{k}_3} \hat{b}_{-\mathbf{k}_2}^\dagger | \Psi_{\mathbf{p}+\mathbf{k}_2}(\omega - \omega_{\mathbf{k}_2}) \rangle \right] \\ &\stackrel{\text{SCBA}}{=} G^{\text{R}*}(\mathbf{p} + \mathbf{q}, \omega + \nu) G^{\text{R}}(\mathbf{p}, \omega) \\ &\cdot \left[1 + \sum_{\mathbf{k}} g(\mathbf{p} + \mathbf{q}, \mathbf{k}) g(\mathbf{p}, \mathbf{k}) \langle \Psi_{\mathbf{p}+\mathbf{q}+\mathbf{k}}^{\text{R}}(\omega + \nu - \omega_{\mathbf{k}}) | \sum_{\mathbf{k}_3} \hat{h}_{\mathbf{p}+\mathbf{q}+\mathbf{k}_3}^\dagger \hat{h}_{\mathbf{p}+\mathbf{k}_3} | \Psi_{\mathbf{p}+\mathbf{k}}(\omega - \omega_{\mathbf{k}}) \rangle \right] \\ &= G^{\text{R}*}(\mathbf{p} + \mathbf{q}, \omega + \nu) G^{\text{R}}(\mathbf{p}, \omega) \cdot \left[1 + \sum_{\mathbf{k}} g(\mathbf{p} + \mathbf{q}, \mathbf{k}) g(\mathbf{p}, \mathbf{k}) N_h^{\text{RR}}(\mathbf{q}, \nu; \mathbf{p} + \mathbf{k}, \omega - \omega_{\mathbf{k}}) \right]. \end{aligned} \quad (\text{S15})$$

In the second equal sign, we use that spin waves are annihilated in the same order as they are created within the SCBA. Effectively, only one order of the Wick contractions is retained. In a similar manner, it follows that

$$N_h^{\text{RA}}(\mathbf{q}, \nu; \mathbf{p}, \omega) = -G^{\text{R}*}(\mathbf{p} + \mathbf{q}, \omega + \nu) G^{\text{A}}(\mathbf{p}, \omega) \cdot \left[1 - \sum_{\mathbf{k}} g(\mathbf{p} + \mathbf{q}, \mathbf{k}) g(\mathbf{p}, \mathbf{k}) N_h^{\text{RA}}(\mathbf{q}, \nu; \mathbf{p} + \mathbf{k}, \omega - \omega_{\mathbf{k}}) \right]. \quad (\text{S16})$$

In this manner, we can iteratively solve for the functions $N_h^{\text{RR}}(\mathbf{q}, \nu; \mathbf{p}, \omega)$ and $N_h^{\text{RA}}(\mathbf{q}, \nu; \mathbf{p}, \omega)$, plug these into Eq. (S14) to calculate $N_h(\mathbf{q}, \nu; \mathbf{p}, \omega)$, which can finally be used in Eq. (S12) to calculate the hole density dynamics.

SHORT-TIME DYNAMICS

In this section, we calculate the short-time dynamics of the hole density dynamics to $\mathcal{O}[(t \cdot \tau)^4]$. To do so, we need to take two spin-wave excitation into account

$$|\Psi_{\mathbf{p}}(\tau)\rangle = C^{(0)}(\mathbf{p}; \tau) \cdot \hat{h}_{\mathbf{p}}^\dagger |\text{AF}\rangle + \sum_{\mathbf{k}} C^{(1)}(\mathbf{p}, \mathbf{k}; \tau) \cdot \hat{h}_{\mathbf{p}+\mathbf{k}}^\dagger \hat{b}_{-\mathbf{k}}^\dagger |\text{AF}\rangle + \sum_{\mathbf{k}, \mathbf{q}} C^{(2)}(\mathbf{p}, \mathbf{k}, \mathbf{q}; \tau) \cdot \hat{h}_{\mathbf{p}+\mathbf{k}+\mathbf{q}}^\dagger \hat{b}_{-\mathbf{q}}^\dagger \hat{b}_{-\mathbf{k}}^\dagger |\text{AF}\rangle \quad (\text{S17})$$

Using the Schrödinger equation, $i\partial_\tau |\Psi_{\mathbf{p}}(\tau)\rangle = H |\Psi_{\mathbf{p}}(\tau)\rangle$, we get

$$\begin{aligned} i\partial_\tau C^{(0)}(\mathbf{p}; \tau) &= \sum_{\mathbf{k}} g(\mathbf{p}, \mathbf{k}) C^{(1)}(\mathbf{p}, \mathbf{k}; \tau), \\ i\partial_\tau C^{(1)}(\mathbf{p}, \mathbf{k}; \tau) &= \omega_{\mathbf{k}} C^{(1)}(\mathbf{p}, \mathbf{k}; \tau) + g(\mathbf{p}, \mathbf{k}) C^{(0)}(\mathbf{p}; \tau) + \sum_{\mathbf{q}} g(\mathbf{p} + \mathbf{k}, \mathbf{q}) C^{(2)}(\mathbf{p}, \mathbf{k}, \mathbf{q}; \tau), \\ i\partial_\tau C^{(2)}(\mathbf{p}, \mathbf{k}; \tau) &= (\omega_{\mathbf{k}} + \omega_{\mathbf{q}}) C^{(2)}(\mathbf{p}, \mathbf{k}; \tau) + g(\mathbf{p} + \mathbf{k}, \mathbf{q}) C^{(1)}(\mathbf{p}, \mathbf{k}; \tau) \end{aligned} \quad (\text{S18})$$

To get an expansion in powers of $t \cdot \tau$, we write

$$\begin{aligned} C^{(0)}(\mathbf{p}; \tau) &= 1 + C_2^{(0)}(\mathbf{p}) \cdot \tau^2 + C_3^{(0)}(\mathbf{p}) \cdot \tau^3 + C_4^{(0)}(\mathbf{p}) \cdot \tau^4, \\ C^{(1)}(\mathbf{p}, \mathbf{k}; \tau) &= C_1^{(1)}(\mathbf{p}, \mathbf{k}) \cdot \tau + C_2^{(1)}(\mathbf{p}, \mathbf{k}) \cdot \tau^2 + C_3^{(1)}(\mathbf{p}, \mathbf{k}) \cdot \tau^3, \\ C^{(2)}(\mathbf{p}, \mathbf{k}, \mathbf{q}; \tau) &= C_2^{(2)}(\mathbf{p}, \mathbf{k}, \mathbf{q}) \cdot \tau^2. \end{aligned} \quad (\text{S19})$$

Generally, at short times, we have $C^{(n)} \propto \tau^n$. The above expansion is enough to get densities that are accurate to fourth order in τ . Looking at the equation of motion for $C^{(0)}(\mathbf{p}; \tau)$, it furthermore follows that the linear term must be absent, $C_1^{(0)} = 0$. Inserting these expression in the equation for $C^{(2)}$ and collecting like powers in τ , we get

$$C_2^{(2)}(\mathbf{p}, \mathbf{k}) = -\frac{i}{2} g(\mathbf{p} + \mathbf{k}, \mathbf{q}) C_1^{(1)}(\mathbf{p}, \mathbf{k}).$$

Likewise, inserting Eq. (S19) into the equation of motion for $C^{(1)}$ yields

$$\begin{aligned} i \left[C_1^{(1)}(\mathbf{p}, \mathbf{k}) + 2\tau \cdot C_2^{(1)}(\mathbf{p}, \mathbf{k}) + 3\tau^2 \cdot C_3^{(1)}(\mathbf{p}, \mathbf{k}) \right] &= \omega_{\mathbf{k}} \left[\tau \cdot C_1^{(1)}(\mathbf{p}, \mathbf{k}) + \tau^2 \cdot C_2^{(1)}(\mathbf{p}, \mathbf{k}) \right] + g(\mathbf{p}, \mathbf{k}) \left[1 + \tau^2 \cdot C_2^{(0)}(\mathbf{p}) \right] \\ &\quad - \frac{i}{2} \sum_{\mathbf{q}} g^2(\mathbf{p} + \mathbf{k}, \mathbf{q}) \cdot \tau^2 \cdot C_1^{(1)}(\mathbf{p}, \mathbf{k}). \end{aligned}$$

Gathering like orders of τ then results in

$$C_1^{(1)}(\mathbf{p}, \mathbf{k}) = -ig(\mathbf{p}, \mathbf{k}), \quad C_2^{(1)}(\mathbf{p}, \mathbf{k}) = -\frac{\omega_{\mathbf{k}}}{2} g(\mathbf{p}, \mathbf{k}), \quad C_3^{(1)}(\mathbf{p}, \mathbf{k}) = \frac{i}{6} g(\mathbf{p}, \mathbf{k}) \left[\omega_{\mathbf{k}}^2 - 2C_2^{(0)}(\mathbf{p}) + g_{\text{tot}}^2(\mathbf{p} + \mathbf{k}) \right].$$

Finally, the equation of motion for $C^{(0)}$ gives

$$i \left[2\tau \cdot C_2^{(0)}(\mathbf{p}) + 3\tau^2 \cdot C_3^{(0)}(\mathbf{p}) + 4\tau^3 \cdot C_4^{(0)}(\mathbf{p}) \right] = \sum_{\mathbf{k}} g(\mathbf{p}, \mathbf{k}) \cdot \left[\tau \cdot C_1^{(1)}(\mathbf{p}, \mathbf{k}) + \tau^2 \cdot C_2^{(1)}(\mathbf{p}, \mathbf{k}) + \tau^3 \cdot C_3^{(1)}(\mathbf{p}, \mathbf{k}) \right].$$

Taking like powers of τ then results in

$$\begin{aligned} C_2^{(0)}(\mathbf{p}) &= -\frac{1}{2} \sum_{\mathbf{k}} g^2(\mathbf{p}, \mathbf{k}) = -\frac{1}{2} g_{\text{tot}}^2(\mathbf{p}), \quad C_3^{(0)}(\mathbf{p}) = -\frac{i}{3} \sum_{\mathbf{k}} g(\mathbf{p}, \mathbf{k}) C_2^{(1)}(\mathbf{p}, \mathbf{k}) = \frac{i}{6} \sum_{\mathbf{k}} g^2(\mathbf{p}, \mathbf{k}) \cdot \omega_{\mathbf{k}}, \\ C_4^{(0)}(\mathbf{p}) &= -\frac{i}{4} \sum_{\mathbf{k}} g(\mathbf{p}, \mathbf{k}) C_3^{(1)}(\mathbf{p}, \mathbf{k}) = \frac{1}{24} \sum_{\mathbf{k}} g^2(\mathbf{p}, \mathbf{k}) \left[\omega_{\mathbf{k}}^2 + g_{\text{tot}}^2(\mathbf{p}) + g_{\text{tot}}^2(\mathbf{p} + \mathbf{k}) \right]. \end{aligned} \quad (\text{S20})$$

Using these expressions, we may then write up the final result for $C_j^{(1)}$

$$C_1^{(1)}(\mathbf{p}, \mathbf{k}) = -ig(\mathbf{p}, \mathbf{k}), \quad C_2^{(1)}(\mathbf{p}, \mathbf{k}) = -\frac{\omega_{\mathbf{k}}}{2} g(\mathbf{p}, \mathbf{k}), \quad C_3^{(1)}(\mathbf{p}, \mathbf{k}) = \frac{i}{6} g(\mathbf{p}, \mathbf{k}) \left[\omega_{\mathbf{k}}^2 + g_{\text{tot}}^2(\mathbf{p}) + g_{\text{tot}}^2(\mathbf{p} + \mathbf{k}) \right], \quad (\text{S21})$$

and $C_2^{(2)}$

$$C_2^{(2)}(\mathbf{p}, \mathbf{k}) = -\frac{1}{2} g(\mathbf{p}, \mathbf{k}) g(\mathbf{p} + \mathbf{k}, \mathbf{q}). \quad (\text{S22})$$

We are now ready to calculate the density to order $(t \cdot \tau)^4$. We utilize that the density may be calculated as an infinite series

$$n_h(\mathbf{d}, \tau) = \sum_{j=0}^{\infty} n_h^{(j)}(\mathbf{d}, \tau). \quad (\text{S23})$$

Here, $n_h^{(j)}$ contains the density contribution from the j 'th order of the state $|\Psi(\tau)\rangle$. The terms are explicitly,

$$\begin{aligned} n_h^{(0)}(\mathbf{d}, \tau) &= \left| \langle \text{AF} | \hat{h}_{\mathbf{d}} | \Psi(\tau) \rangle \right|^2 = \left| \frac{1}{N} \sum_{\mathbf{p}} e^{i\mathbf{p} \cdot \mathbf{d}} C^{(0)}(\mathbf{p}; \tau) \right|^2, \\ n_h^{(1)}(\mathbf{d}, \tau) &= \sum_{\mathbf{k}} \left| \langle \text{AF} | \hat{b}_{-\mathbf{k}} \hat{h}_{\mathbf{d}} | \Psi(\tau) \rangle \right|^2 = \sum_{\mathbf{k}} \left| \frac{1}{N} \sum_{\mathbf{p}} e^{i\mathbf{p} \cdot \mathbf{d}} C^{(1)}(\mathbf{p}, \mathbf{k}; \tau) \right|^2, \\ n_h^{(2)}(\mathbf{d}, \tau) &= \sum_{\mathbf{k}, \mathbf{q}} \left| \langle \text{AF} | \hat{b}_{-\mathbf{k}} \hat{b}_{-\mathbf{q}} \hat{h}_{\mathbf{d}} | \Psi(\tau) \rangle \right|^2 = \sum_{\mathbf{k}, \mathbf{q}} \left| \frac{1}{N} \sum_{\mathbf{p}} e^{i\mathbf{p} \cdot \mathbf{d}} C^{(2)}(\mathbf{p}, \mathbf{k}, \mathbf{q}; \tau) \right|^2, \end{aligned} \quad (\text{S24})$$

and so on for higher orders. Defining $C_j^{(n)}(\mathbf{d}, \dots) = N^{-1} \sum_{\mathbf{p}} e^{i\mathbf{p} \cdot \mathbf{d}} C^{(n)}(\mathbf{p}, \dots)$, we may then write

$$\begin{aligned} n_h^{(0)}(\mathbf{d}, \tau) &= \left| C_0^{(0)}(\mathbf{d}) + C_2^{(0)}(\mathbf{d}) \cdot \tau^2 + C_3^{(0)}(\mathbf{d}) \cdot \tau^3 + C_4^{(0)}(\mathbf{d}) \cdot \tau^4 \right|^2 + \mathcal{O}[(t \cdot \tau)^5] \\ &= \left| C_0^{(0)}(\mathbf{d}) \right|^2 + 2\text{Re} \left[C_2^{(0)*}(\mathbf{d}) C_0^{(0)}(\mathbf{d}) \right] \cdot \tau^2 + 2\text{Re} \left[C_3^{(0)*}(\mathbf{d}) C_0^{(0)}(\mathbf{d}) \right] \cdot \tau^3 \\ &\quad + \left(\left| C_2^{(0)}(\mathbf{d}) \right|^2 + 2\text{Re} \left[C_4^{(0)*}(\mathbf{d}) C_0^{(0)}(\mathbf{d}) \right] \right) \cdot \tau^4 + \mathcal{O}[(t \cdot \tau)^5] \\ &= n_{h,0}^{(0)}(\mathbf{d}) + n_{h,2}^{(0)}(\mathbf{d}) \cdot (t \cdot \tau)^2 + n_{h,3}^{(0)}(\mathbf{d}) \cdot (t \cdot \tau)^3 + n_{h,4}^{(0)}(\mathbf{d}) \cdot (t \cdot \tau)^4 + \mathcal{O}[(t \cdot \tau)^5]. \end{aligned} \quad (\text{S25})$$

Likewise,

$$\begin{aligned} n_h^{(1)}(\mathbf{d}, \tau) &= \sum_{\mathbf{k}} \left| C_1^{(1)}(\mathbf{d}, \mathbf{k}) \cdot \tau + C_2^{(1)}(\mathbf{d}, \mathbf{k}) \cdot \tau^2 + C_3^{(1)}(\mathbf{d}, \mathbf{k}) \cdot \tau^3 \right|^2 + \mathcal{O}[(t \cdot \tau)^5] \\ &= \sum_{\mathbf{k}} \left(\left| C_1^{(1)}(\mathbf{d}, \mathbf{k}) \right|^2 \cdot \tau^2 + 2\text{Re} \left[C_2^{(1)*}(\mathbf{d}, \mathbf{k}) C_1^{(1)}(\mathbf{d}, \mathbf{k}) \right] \cdot \tau^3 \right. \\ &\quad \left. + \left(\left| C_2^{(1)}(\mathbf{d}, \mathbf{k}) \right|^2 + 2\text{Re} \left[C_3^{(1)*}(\mathbf{d}, \mathbf{k}) C_1^{(1)}(\mathbf{d}, \mathbf{k}) \right] \right) \cdot \tau^4 \right) + \mathcal{O}[(t \cdot \tau)^5] \\ &= n_{h,2}^{(1)}(\mathbf{d}) \cdot (t \cdot \tau)^2 + n_{h,3}^{(1)}(\mathbf{d}) \cdot (t \cdot \tau)^3 + n_{h,4}^{(1)}(\mathbf{d}) \cdot (t \cdot \tau)^4 + \mathcal{O}[(t \cdot \tau)^5]. \end{aligned} \quad (\text{S26})$$

From second order in the wave function,

$$n_h^{(2)}(\mathbf{d}, \tau) = \sum_{\mathbf{k}, \mathbf{q}} \left| C_2^{(2)}(\mathbf{d}, \mathbf{k}, \mathbf{q}) \right|^2 \cdot \tau^4 + \mathcal{O}[(t \cdot \tau)^5] = n_{h,4}^{(2)}(\mathbf{d}) \cdot (t \cdot \tau)^4 + \mathcal{O}[(t \cdot \tau)^5]. \quad (\text{S27})$$

We, finally, reorganize the terms in $n_h(\mathbf{d}, \tau) \simeq n_h^{(0)}(\mathbf{d}, \tau) + n_h^{(1)}(\mathbf{d}, \tau) + n_h^{(2)}(\mathbf{d}, \tau)$ according to their order in $(t \cdot \tau)$. This gives

$$n_h(\mathbf{d}, \tau) \simeq n_{h,0}^{(0)}(\mathbf{d}) + \left[n_{h,2}^{(0)}(\mathbf{d}) + n_{h,2}^{(1)}(\mathbf{d}) \right] \cdot (t \cdot \tau)^2 + \left[n_{h,4}^{(0)}(\mathbf{d}) + n_{h,4}^{(1)}(\mathbf{d}) + n_{h,4}^{(2)}(\mathbf{d}) \right] \cdot (t \cdot \tau)^4. \quad (\text{S28})$$

Here, we utilize that the 3rd order terms proportional to $(t \cdot \tau)^3$ all vanish identically, as the exterior of the real values $\text{Re}[\dots]$ turn out to be purely imaginary. We can now write out the explicit terms related to each order. At 0th order in time, we simply have

$$n_{h,0}^{(0)}(\mathbf{d}) = \left| C_2^{(0)}(\mathbf{d}) \right|^2 = \delta_{d,0}. \quad (\text{S29})$$

At 2nd order, we get

$$n_{h,2}^{(0)}(\mathbf{d}) = \frac{2}{t^2} \text{Re} \left[C_2^{(0)*}(\mathbf{d}) C_0^{(0)}(\mathbf{d}) \right] = -\delta_{d,0} \cdot \frac{1}{N t^2} \sum_{\mathbf{p}} g_{\text{tot}}^2(\mathbf{p}) \simeq -\delta_{d,0} \cdot 3.37. \quad (\text{S30})$$

The numerical value is in the Heisenberg limit, $\alpha \rightarrow 1$, evaluated for a 20×20 lattice. Further,

$$n_{h,2}^{(1)}(\mathbf{d}) = \frac{1}{t^2} \sum_{\mathbf{k}} \left| C_1^{(1)}(\mathbf{d}, \mathbf{k}) \right|^2 = \frac{1}{t^2} \sum_{\mathbf{k}} \left| \frac{1}{N} \sum_{\mathbf{p}} e^{i\mathbf{p} \cdot \mathbf{d}} g(\mathbf{p}, \mathbf{k}) \right|^2 = \delta_{d,1} \cdot \frac{1}{N} \sum_{\mathbf{k}} |u_{\mathbf{k}} e^{-i\mathbf{k} \cdot \mathbf{d}} - v_{\mathbf{k}}|^2 \simeq \delta_{d,1} \cdot 0.843. \quad (\text{S31})$$

Here, we use that $g(\mathbf{p}, \mathbf{k}) = zt(u_{\mathbf{k}}\gamma_{\mathbf{p}+\mathbf{k}} - v_{\mathbf{k}}\gamma_{\mathbf{p}})/\sqrt{N}$, and that $\gamma_{\mathbf{q}} = \sum_{\boldsymbol{\delta}} e^{i\mathbf{q} \cdot \boldsymbol{\delta}}/z$, to explicitly evaluate the \mathbf{p} sum. Again, the numerical value is for the Heisenberg limit. The 0th fourth order term evaluates to

$$\begin{aligned} n_{h,4}^{(0)}(\mathbf{d}) &= \frac{1}{t^4} \left(\left| C_2^{(0)}(\mathbf{d}) \right|^2 + 2\text{Re} \left[C_4^{(0)*}(\mathbf{d}) C_0^{(0)}(\mathbf{d}) \right] \right) \\ &= \frac{1}{t^4} \left(\frac{1}{4} \left| \frac{1}{N} \sum_{\mathbf{p}} e^{i\mathbf{p} \cdot \mathbf{d}} g_{\text{tot}}^2(\mathbf{p}) \right|^2 + \frac{\delta_{d,0}}{12} \cdot \frac{1}{N} \sum_{\mathbf{p}, \mathbf{k}} g^2(\mathbf{p}, \mathbf{k}) [\omega_{\mathbf{k}}^2 + g_{\text{tot}}^2(\mathbf{p}) + g_{\text{tot}}^2(\mathbf{p} + \mathbf{k})] \right) \\ &\simeq \delta_{d,0} \left[0.917 \cdot \left(\frac{J}{t} \right)^2 + 4.522 \right] + \delta_{d,\sqrt{2}} \cdot 0.044 + \delta_{d,2} \cdot 0.014 \end{aligned} \quad (\text{S32})$$

The 1st fourth order term is, similarly,

$$\begin{aligned} n_{h,4}^{(1)}(\mathbf{d}) &= \frac{1}{t^4} \sum_{\mathbf{k}} \left(\left| C_2^{(1)}(\mathbf{d}, \mathbf{k}) \right|^2 + 2\text{Re} \left[C_3^{(1)*}(\mathbf{d}, \mathbf{k}) C_1^{(1)}(\mathbf{d}, \mathbf{k}) \right] \right) \\ &= \frac{1}{Nt^2} \sum_{\mathbf{k}} \delta_{d,1} \cdot \left(\frac{\omega_{\mathbf{k}}^2}{4} |u_{\mathbf{k}} e^{-i\mathbf{k} \cdot \mathbf{d}} - v_{\mathbf{k}}|^2 - \frac{1}{3} \text{Re} \left[(u_{\mathbf{k}} e^{-i\mathbf{k} \cdot \mathbf{d}} - v_{\mathbf{k}}) \cdot \frac{1}{t\sqrt{N}} \sum_{\mathbf{p}} e^{-i\mathbf{p} \cdot \mathbf{d}} g(\mathbf{p}, \mathbf{k}) [\omega_{\mathbf{k}}^2 + g_{\text{tot}}^2(\mathbf{p}) + g_{\text{tot}}^2(\mathbf{p} + \mathbf{k})] \right] \right) \\ &= \frac{1}{Nt^2} \sum_{\mathbf{k}} \delta_{d,1} \cdot \left(-\frac{\omega_{\mathbf{k}}^2}{12} |u_{\mathbf{k}} e^{-i\mathbf{k} \cdot \mathbf{d}} - v_{\mathbf{k}}|^2 - \frac{1}{3} \text{Re} \left[(u_{\mathbf{k}} e^{-i\mathbf{k} \cdot \mathbf{d}} - v_{\mathbf{k}}) \cdot \frac{1}{t\sqrt{N}} \sum_{\mathbf{p}} e^{-i\mathbf{p} \cdot \mathbf{d}} g(\mathbf{p}, \mathbf{k}) [g_{\text{tot}}^2(\mathbf{p}) + g_{\text{tot}}^2(\mathbf{p} + \mathbf{k})] \right] \right) \\ &\simeq \frac{\delta_{d,1}}{4} \left[-0.917 \left(\frac{J}{t} \right)^2 - 6.746 \right] \end{aligned} \quad (\text{S33})$$

Finally,

$$\begin{aligned} n_{h,4}^{(2)}(\mathbf{d}) &= \frac{1}{t^4} \sum_{\mathbf{k}, \mathbf{q}} \left| C_2^{(2)}(\mathbf{d}, \mathbf{k}) \right|^2 = \frac{1}{4t^4} \sum_{\mathbf{k}, \mathbf{q}} \left| \frac{1}{N} \sum_{\mathbf{p}} e^{i\mathbf{p} \cdot \mathbf{d}} g(\mathbf{p}, \mathbf{k}) g(\mathbf{p} + \mathbf{k}, \mathbf{q}) \right|^2 \\ &= \delta_{d,0} \cdot 0.196 + \delta_{d,\sqrt{2}} \cdot 0.272 + \delta_{d,2} \cdot 0.177 \end{aligned} \quad (\text{S34})$$

We are now ready to characterize the short-time motion of the hole up to order $(t \cdot \tau)^4$. To this end, we calculate the root-mean-square distance

$$\begin{aligned} d_{\text{rms}} &= \left[\sum_{\mathbf{d}} d^2 n_h(\mathbf{d}, \tau) \right]^{1/2} \simeq \left[\sum_{\mathbf{d}} d^2 \left(n_{h,0}^{(0)}(\mathbf{d}) + [n_{h,2}^{(0)}(\mathbf{d}) + n_{h,2}^{(1)}(\mathbf{d})] (t \cdot \tau)^2 + [n_{h,4}^{(0)}(\mathbf{d}) + n_{h,4}^{(1)}(\mathbf{d}) + n_{h,4}^{(2)}(\mathbf{d})] (t \cdot \tau)^4 \right) \right]^{1/2} \\ &= v_{\text{rms}}^0 \cdot \tau [1 - c_3 \cdot (t \cdot \tau)^2] + \mathcal{O}[(t \cdot \tau)^5] \end{aligned} \quad (\text{S35})$$

Here,

$$v_{\text{rms}}^0 = 2t \cdot \left[\frac{1}{N} \sum_{\mathbf{k}} |u_{\mathbf{k}} e^{-i\mathbf{k} \cdot \mathbf{d}} - v_{\mathbf{k}}|^2 \right]^{1/2} \simeq 1.835t, \quad (\text{S36})$$

is the initial expansion velocity for the hole. Compared to a free quantum walk of a particle, this has a correction factor of $[\frac{1}{N} \sum_{\mathbf{k}} |u_{\mathbf{k}} e^{-i\mathbf{k} \cdot \mathbf{d}} - v_{\mathbf{k}}|^2]^{1/2} \simeq 0.918$ in the Heisenberg limit, $\alpha \rightarrow 1$. This is fundamentally due to the nonzero spin fluctuations in the antiferromagnetic quantum ground state. Furthermore,

$$c_3 = -\frac{4n_{h,4}^{(1)}(d=1) + 4(2n_{h,4}^{(2)}(d=\sqrt{2}) + 4n_{h,4}^{(2)}(d=2))}{2(v_{\text{rms}}^0/t)^2} = c_3^{(0)} + c_3^{(J)} \cdot \left(\frac{J}{t} \right)^2 \simeq 0.172 + 0.136 \cdot \left(\frac{J}{t} \right)^2, \quad (\text{S37})$$

gives the lowest order correction to the initial ballistic motion. Again, the numerical values are for the Heisenberg case in a 2D antiferromagnet. Note that this depends on the inverse interaction strength squared, $(J/t)^2$. In particular, we can use it to define the timescale for when the initial ballistic motion breaks down, by setting $1 - c_3 \cdot (t \cdot \tau_s)^2 = 1/2$. This yields Eq. (8) of the main text.

ASYMPTOTIC POLARON DYNAMICS

In this section, we analyze the asymptotic dynamics of the expansion coefficients in $|\Psi_{\mathbf{p}}(\tau)\rangle$

$$|\Psi_{\mathbf{p}}(\tau)\rangle = C^{(0)}(\mathbf{p}; \tau) \cdot \hat{h}_{\mathbf{p}}^{\dagger} |\text{AF}\rangle + \sum_{\mathbf{k}_1} C^{(1)}(\mathbf{p}, \mathbf{k}_1; \tau) \cdot \hat{h}_{\mathbf{p}+\mathbf{k}_1}^{\dagger} \hat{b}_{-\mathbf{k}_1}^{\dagger} |\text{AF}\rangle + \dots \quad (\text{S38})$$

to all orders, and show that this is solely governed by polaron dynamics. Since $|\Psi_{\mathbf{p}}(\tau)\rangle$ is the Fourier transform of $|\Psi_{\mathbf{p}}(\omega)\rangle = |\Psi_{\mathbf{p}}^{\text{R}}(\omega)\rangle + |\Psi_{\mathbf{p}}^{\text{A}}(\omega)\rangle$, it follows that

$$C^{(n)}(\mathbf{p}, \{\mathbf{k}_j\}; \tau) = \int \frac{d\omega}{2\pi} e^{-i\omega\tau} \cdot 2\text{Re} \left[R^{(n)}(\mathbf{p}, \{\mathbf{k}_j\}; \omega) \right]. \quad (\text{S39})$$

Here, we also use that $|\Psi_{\mathbf{p}}^{\text{A}}(\omega)\rangle = [|\Psi_{\mathbf{p}}^{\text{R}}(\omega)\rangle]^*$. Before we dive into the general case, let us look at the simplest case of order $n = 0$. Here, we get

$$C^{(0)}(\mathbf{p}; \tau) = - \int \frac{d\omega}{2\pi} e^{-i\omega\tau} \cdot 2\text{Im} [G^{\text{R}}(\mathbf{p}, \omega)] = \int \frac{d\omega}{2\pi} e^{-i\omega\tau} \cdot A(\mathbf{p}, \omega), \quad (\text{S40})$$

with $A(\mathbf{p}, \omega) = -2\text{Im}[G^{\text{R}}(\mathbf{p}, \omega)]$ the hole spectral function. Importantly, this has a single well-defined peak at the quasiparticle energy $\varepsilon_{\mathbf{p}} = \Sigma(\mathbf{p}, \varepsilon_{\mathbf{p}})$, i.e. $A(\mathbf{p}, \omega \sim \varepsilon_{\mathbf{p}}) = 2\pi Z_{\mathbf{p}} \cdot \delta(\omega - \varepsilon_{\mathbf{p}})$, with $Z_{\mathbf{p}}$ the quasiparticle residue. At long times, this pole is the only remaining contribution, and, therefore,

$$C^{(0)}(\mathbf{p}; \tau) = \int \frac{d\omega}{2\pi} e^{-i\omega\tau} \cdot A(\mathbf{p}, \omega) \rightarrow Z_{\mathbf{p}} \cdot e^{-i\varepsilon_{\mathbf{p}}\tau}. \quad (\text{S41})$$

This is the principle line of reasoning, we will use in the following. In the general case, we utilize the recursion relation in Eq. (S6) as well as the explicit coefficients in Eq. (S9). To make the calculations more concise in the following, we let $G^{\text{R}}(\mathbf{K}_n) = G^{\text{R}}(\mathbf{K}_n, \omega - \sum_{l=1}^n \omega_{\mathbf{k}_l})$, $A(\mathbf{K}_n) = A(\mathbf{K}_n, \omega - \sum_{l=1}^n \omega_{\mathbf{k}_l})$, and $C^{(n)} = C^{(n)}(\mathbf{p}, \{\mathbf{k}_j\}_1^n; \omega)$, $R^{(n)} = R^{(n)}(\mathbf{p}, \{\mathbf{k}_j\}_1^n; \omega)$. We, thus, obtain

$$\begin{aligned} C^{(n)} &= 2\text{Re} [R^{(n)}] = 2g(\mathbf{K}_{n-1}, \mathbf{k}_n) \text{Re} [G^{\text{R}}(\mathbf{K}_n) R^{(n-1)}] \\ &= 2g(\mathbf{K}_{n-1}, \mathbf{k}_n) \left\{ \text{Re}[G^{\text{R}}(\mathbf{K}_n)] \text{Re}[R^{(n-1)}] - \text{Im}[G^{\text{R}}(\mathbf{K}_n)] \text{Im}[R^{(n-1)}] \right\} \\ &= g(\mathbf{K}_{n-1}, \mathbf{k}_n) \left\{ \text{Re}[G^{\text{R}}(\mathbf{K}_n)] C^{(n-1)} + A(\mathbf{K}_n) \text{Im}[R^{(n-1)}] \right\} \\ &= \text{Re} \left[G^{\text{R}}(\mathbf{K}_0) \cdot \prod_{j=1}^{n-1} g(\mathbf{K}_{j-1}, \mathbf{k}_j) G^{\text{R}}(\mathbf{K}_j) \right] \cdot g(\mathbf{K}_{n-1}, \mathbf{k}_n) A(\mathbf{K}_n) + g(\mathbf{K}_{n-1}, \mathbf{k}_n) \text{Re}[G^{\text{R}}(\mathbf{K}_n)] C^{(n-1)}. \end{aligned} \quad (\text{S42})$$

In the second line, we utilize that the real part of a product of complex numbers is the product of the real parts minus the product of the imaginary parts. In the last line, we use that $\text{Im}[R^{(n-1)}] = \text{Re}[-iR^{(n-1)}] = \text{Re}[G^{\text{R}}(\mathbf{K}_0) \cdot \prod_{j=1}^{n-1} g(\mathbf{K}_{j-1}, \mathbf{k}_j) G^{\text{R}}(\mathbf{K}_j)]$. Using this relation n times yields (in which we now write out all terms explicitly)

$$\begin{aligned} C^{(n)}(\mathbf{p}, \{\mathbf{k}_j\}_1^n; \omega) &= \prod_{j=1}^n g(\mathbf{K}_{j-1}, \mathbf{k}_j) \left\{ A(\mathbf{p}, \omega) \prod_{j=1}^n \text{Re}[G^{\text{R}}(\mathbf{K}_j, \omega - \sum_{l=1}^j \omega_{\mathbf{k}_l})] \right. \\ &\quad \left. + \sum_{m=1}^n A(\mathbf{K}_m, \omega - \sum_{l=1}^m \omega_{\mathbf{k}_l}) \cdot \text{Re} \left[G^{\text{R}}(\mathbf{p}, \omega) \prod_{j=1}^{m-1} G^{\text{R}}(\mathbf{K}_j, \omega - \sum_{l=1}^j \omega_{\mathbf{k}_l}) \right] \cdot \prod_{j=m+1}^n \text{Re} \left[G^{\text{R}}(\mathbf{K}_j, \omega - \sum_{l=1}^j \omega_{\mathbf{k}_l}) \right] \right\}. \end{aligned} \quad (\text{S43})$$

Importantly, this expression is now in the form of products of terms in which only a single quasiparticle pole appears. Specifically, terms like $\prod \text{Re}[G^{\text{R}}(\mathbf{K}_j, \omega - \sum_{l=1}^j \omega_{\mathbf{k}_l})]$ contain no poles, as only the real part of the Green's functions appear. Also, the term $\text{Re}[G^{\text{R}}(\mathbf{p}, \omega) \prod_{j=1}^{m-1} G^{\text{R}}(\mathbf{K}_j, \omega - \sum_{l=1}^j \omega_{\mathbf{k}_l})]$ have poles $\varepsilon_{\mathbf{K}_j} + \sum_{l=1}^j \omega_{\mathbf{k}_l}$, but these all lie below the first pole of $A(\mathbf{K}_m, \omega - \sum_{l=1}^m \omega_{\mathbf{k}_l})$ at $\varepsilon_{\mathbf{K}_j} + \sum_{l=1}^m \omega_{\mathbf{k}_l}$. Therefore, only the latter pole contributes to the long time

dynamics in these terms. In total, then, we may write down the explicitly asymptotic limit of the Fourier transform

$$C^{(n)}(\mathbf{p}, \{\mathbf{k}_j\}_1^n; \tau) = \prod_{j=1}^n g(\mathbf{K}_{j-1}, \mathbf{k}_j) \left\{ Z_{\mathbf{p}} e^{-i\varepsilon_{\mathbf{p}}\tau} \prod_{j=1}^n G^{\text{R}}(\mathbf{K}_j, \varepsilon_{\mathbf{p}} - \sum_{l=1}^j \omega_{\mathbf{k}_l}) + \sum_{m=1}^n Z_{\mathbf{K}_m} e^{-i(\varepsilon_{\mathbf{K}_m} + \sum_{l=1}^m \omega_{\mathbf{k}_l})\tau} \right. \\ \left. \times \text{Re} \left[G^{\text{R}}(\mathbf{p}, \varepsilon_{\mathbf{K}_m} + \sum_{l=1}^m \omega_{\mathbf{k}_l}) \prod_{j=1}^{m-1} G^{\text{R}}(\mathbf{K}_j, \varepsilon_{\mathbf{K}_m} + \sum_{l=j+1}^m \omega_{\mathbf{k}_l}) \right] \prod_{j=m+1}^n G^{\text{R}}(\mathbf{K}_j, \varepsilon_{\mathbf{K}_m} - \sum_{l=m+1}^j \omega_{\mathbf{k}_l}) \right\}. \quad (\text{S44})$$

Here, we use that in terms like $\text{Re}[G^{\text{R}}(\mathbf{K}_j, \varepsilon_{\mathbf{p}} - \sum_{l=1}^j \omega_{\mathbf{k}_l})]$, the Green's function is evaluated below the quasiparticle pole, and is, therefore, already real. Inserting this expression into Eq. (S38), and grouping terms with respect to the overall factor of the residue, we see that

$$|\Psi_{\mathbf{p}}(\tau)\rangle = Z_{\mathbf{p}} e^{-i\varepsilon_{\mathbf{p}}\tau} \left[\hat{h}_{\mathbf{p}}^{\dagger} + \sum_{n=1}^{\infty} \sum_{\{\mathbf{k}_j\}_1^n} \hat{h}_{\mathbf{K}_n}^{\dagger} \prod_{j=1}^n g(\mathbf{K}_{j-1}, \mathbf{k}_j) G^{\text{R}}(\mathbf{K}_j, \varepsilon_{\mathbf{p}} - \sum_{l=1}^j \omega_{\mathbf{k}_l}) \hat{b}_{-\mathbf{k}_j}^{\dagger} \right] |\text{AF}\rangle \\ + \sum_{\mathbf{k}_1} g(\mathbf{p}, \mathbf{k}_1) \text{Re}[G^{\text{R}}(\mathbf{p}, \varepsilon_{\mathbf{K}_1} + \omega_{\mathbf{k}_1})] Z_{\mathbf{K}_1} e^{-i(\varepsilon_{\mathbf{K}_1} + \omega_{\mathbf{k}_1})\tau} \hat{b}_{-\mathbf{k}_1}^{\dagger} \\ \cdot \left[\hat{h}_{\mathbf{K}_1}^{\dagger} + \sum_{n=2}^{\infty} \sum_{\{\mathbf{k}_j\}_2^n} \hat{h}_{\mathbf{K}_n}^{\dagger} \prod_{j=2}^n g(\mathbf{K}_{j-1}, \mathbf{k}_j) G^{\text{R}}(\mathbf{K}_j, \varepsilon_{\mathbf{K}_1} - \sum_{l=2}^j \omega_{\mathbf{k}_l}) \hat{b}_{-\mathbf{k}_j}^{\dagger} \right] |\text{AF}\rangle + \dots \quad (\text{S45})$$

In this way, we have managed to write the asymptotic dynamics solely in terms of the magnetic polaron states [1, 2, 7]

$$|\Psi_{\mathbf{p}}^{\text{pol}}\rangle = \sqrt{Z_{\mathbf{p}}} \left[\hat{h}_{\mathbf{p}}^{\dagger} + \sum_{n=1}^{\infty} \sum_{\{\mathbf{k}_j\}_1^n} \hat{h}_{\mathbf{K}_n}^{\dagger} \prod_{j=1}^n g(\mathbf{K}_{j-1}, \mathbf{k}_j) G^{\text{R}}(\mathbf{K}_j, \varepsilon_{\mathbf{p}} - \sum_{l=1}^j \omega_{\mathbf{k}_l}) \hat{b}_{-\mathbf{k}_j}^{\dagger} \right] |\text{AF}\rangle. \quad (\text{S46})$$

Explicitly,

$$|\Psi_{\mathbf{p}}(\tau)\rangle = \sqrt{Z_{\mathbf{p}}} e^{-i\varepsilon_{\mathbf{p}}\tau} |\Psi_{\mathbf{p}}^{\text{pol}}\rangle \\ + \sum_{n=1}^{\infty} \sum_{\{\mathbf{k}_j\}_1^n} \text{Re} \left[\prod_{j=1}^n g(\mathbf{K}_{j-1}, \mathbf{k}_j) G^{\text{R}}(\mathbf{K}_{j-1}, \varepsilon_{\mathbf{K}_n} + \sum_{l=j}^n \omega_{\mathbf{k}_l}) \right] \cdot \sqrt{Z_{\mathbf{K}_n}} e^{-i(\varepsilon_{\mathbf{K}_n} + \sum_{l=1}^n \omega_{\mathbf{k}_l})\tau} \cdot \prod_{j=1}^n \hat{b}_{-\mathbf{k}_j}^{\dagger} |\Psi_{\mathbf{K}_n}^{\text{pol}}\rangle. \quad (\text{S47})$$

This shows that the long time behavior is determined solely by magnetic polarons with $0, 1, \dots$ spin waves on top.

PERTURBATIVE LIMIT

In this section, we calculate the polaron energy bandwidth w_{pol} and asymptotic expansion velocity v_{rms}^{∞} in the perturbative limit to order t^2/J . First, we calculate the polaron energy to order t^2/J by using the self-energy $\Sigma(\mathbf{p}, \omega)$ to lowest order in the interaction [See Eq. (4) of the main text]

$$\varepsilon_{\mathbf{p}}^{(0)} = \Sigma^{(0)}(\mathbf{p}, 0) = - \sum_{\mathbf{k}} \frac{g^2(\mathbf{p}, \mathbf{k})}{\omega_{\mathbf{k}}} = - \frac{t^2}{J} \sum_{\mathbf{k}} \frac{\tilde{g}^2(\mathbf{p}, \mathbf{k})}{\tilde{\omega}_{\mathbf{k}}}. \quad (\text{S48})$$

Here, $\tilde{g} = g/t$ and $\tilde{\omega}_{\mathbf{k}} = \omega_{\mathbf{k}}/J$. From this, it is straightforward to get the perturbative polaron bandwidth as

$$w_{\text{pol}}^{(0)} = \varepsilon_{\mathbf{0}}^{(0)} - \varepsilon_{(\pi/2, \pi/2)}^{(0)} = c_w(\alpha) \frac{t^2}{J}. \quad (\text{S49})$$

Numerically, we determine $c_w(\alpha \rightarrow 1) \simeq 1.97$ for a square lattice of size 20×20 . To calculate the asymptotic expansion velocity, we need the mean-square distance

$$d_{\text{rms}}^2 = \sum_{\mathbf{d}} d^2 \langle \Psi(\tau) | \hat{h}_{\mathbf{d}}^{\dagger} \hat{h}_{\mathbf{d}} | \Psi(\tau) \rangle = \sum_{\mathbf{p}} \langle \Psi(\tau) | \hat{h}_{\mathbf{d}}^{\dagger} (-\nabla_{\mathbf{p}}^2) \hat{h}_{\mathbf{p}} | \Psi(\tau) \rangle. \quad (\text{S50})$$

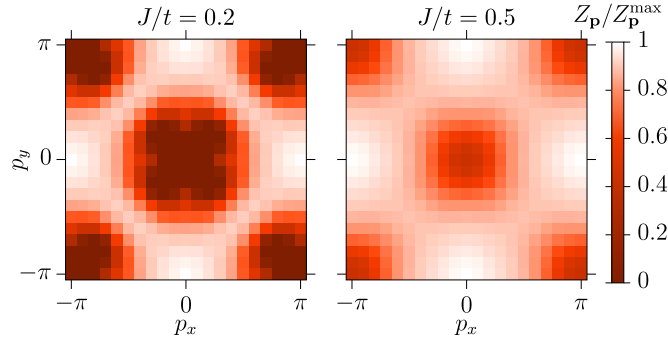


FIG. S2. Quasiparticle residue for two indicated interactions strengths. This has been normalized to the maximal residue at each interaction strength to highlight differences in the residue across the Brillouin zone. For the strongly interacting case (left), the residue becomes vanishingly small in the center and corners of the Brillouin zone, constituting a clear qualitative difference to the behavior at moderate interactions (right).

From the previous section, we get the long time behavior of $|\Psi_{\mathbf{p}}(\tau)\rangle$ up to first order in spin waves

$$|\Psi_{\mathbf{p}}(\tau)\rangle = Z_{\mathbf{p}} e^{-i\varepsilon_{\mathbf{p}}\tau} \hat{h}_{\mathbf{p}}^{\dagger} |\text{AF}\rangle + \sum_{\mathbf{k}} g(\mathbf{p}, \mathbf{k}) \left\{ Z_{\mathbf{p}} e^{-i\varepsilon_{\mathbf{p}}\tau} G^{\text{R}}(\mathbf{p} + \mathbf{k}, \varepsilon_{\mathbf{p}} - \omega_{\mathbf{k}}) + Z_{\mathbf{p}+\mathbf{k}} e^{-i(\varepsilon_{\mathbf{p}+\mathbf{k}} + \omega_{\mathbf{k}})\tau} \text{Re} [G^{\text{R}}(\mathbf{p}, \varepsilon_{\mathbf{p}+\mathbf{k}} + \omega_{\mathbf{k}})] \right\} \hat{h}_{\mathbf{p}+\mathbf{k}}^{\dagger} \hat{b}_{-\mathbf{k}}^{\dagger} |\text{AF}\rangle. \quad (\text{S51})$$

In principle, we, then, need to calculate the double derivative of this full expression with respect to momentum. However, at long times, only terms in which the phases are derived with respect to time contribute significantly, since they will scale as τ^2 . The lowest order result for the mean-square distance at long times is, therefore, simply

$$d_{\text{rms}}^2 \rightarrow \tau^2 \frac{1}{N} \sum_{\mathbf{p}} (\nabla_{\mathbf{p}} \varepsilon_{\mathbf{p}}^{(0)})^2 = c_v^2(\alpha) \cdot \left(\frac{t^2}{J} \right)^2 \tau^2, \quad (\text{S52})$$

replacing $\varepsilon_{\mathbf{p}}$ with $\varepsilon_{\mathbf{p}}^{(0)}$ in Eq. (S51). Hence, $v_{\text{rms}}^{\infty} = c_v \cdot t^2/J$. Using Eq. (S48), we get

$$c_v^2(\alpha) = \frac{2^4}{N^2} \sum_{\mathbf{p}, \mathbf{q}, \mathbf{k}} \frac{\tilde{g}(\mathbf{p}, \mathbf{q}) \tilde{g}(\mathbf{p}, \mathbf{k})}{\tilde{\omega}_{\mathbf{k}} \tilde{\omega}_{\mathbf{q}}} \left\{ [u_{\mathbf{k}} \sin(p_x + k_x) - v_{\mathbf{k}} \sin(p_x)] [u_{\mathbf{q}} \sin(p_x + q_x) - v_{\mathbf{q}} \sin(p_x)] \right. \\ \left. + [u_{\mathbf{k}} \sin(p_y + k_y) - v_{\mathbf{k}} \sin(p_y)] [u_{\mathbf{q}} \sin(p_y + q_y) - v_{\mathbf{q}} \sin(p_y)] \right\}. \quad (\text{S53})$$

Numerically, we, hereby, determine $c_v(\alpha \rightarrow 1) = 0.81$ for a square lattice of size 20×20 . This yields the perturbative limit of the ratio

$$\frac{v_{\text{rms}}^{\infty}}{w_{\text{pol}}} = \frac{c_v}{c_w} \simeq 0.41, \quad (\text{S54})$$

where the numerical value is in the Heisenberg limit of $\alpha = 1$. We have checked the finite size dependency of this ratio, which seems to be within 0.1%. As mentioned in connection with Fig. 4 of the main text, the relation in Eq. (S54) remains roughly constant until $J \lesssim 0.4t$, where $v_{\text{rms}}^{\infty}/w_{\text{pol}}$ suddenly starts to drop. We associated this with a qualitative change in the behavior of the quasiparticle residue throughout the Brillouin zone. We elucidate this in more detail in S2, in which the residue is plotted as a heat map for two indicated interactions strengths. In the strongly interacting case of $J = 0.2t$, the residue becomes vanishingly small in the center and corners of the Brillouin zone, whereby these states cannot efficiently contribute to the long-time dynamics of the moving hole.

ENERGY AND LIFETIME OF LOWEST STRING EXCITATION

In this section, we show our numerical evidence for the presence of the lowest string excitation, see Figs. 3(e) and 3(f) of the main text. To extract these, we perform a Lorentzian fit

$$L(Z, E, \Gamma; \omega) = 2Z \frac{1/\tau}{(\omega - E)^2 + (1/\tau)^2}, \quad (\text{S55})$$

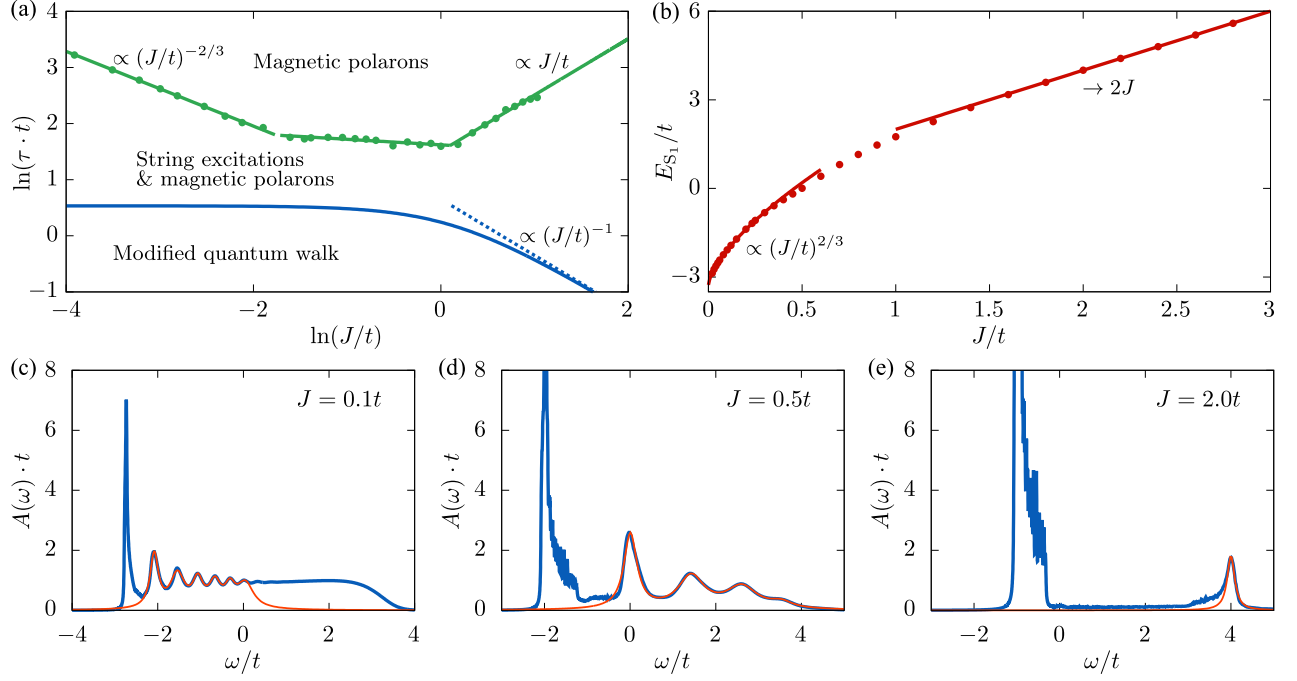


FIG. S3. (a) Extracted lifetime [green points] along with power-law fits (green solid lines) of the lowest string excitation, S_1 . For better comparison with Fig. 1(c) of the main text, we also show τ_s [Eq. (8) of the main text]. (b) Associated energy of the lowest energy string excitation (red points) along with power-law fits in the strong ($J \ll t$) and weak ($J \gg t$) coupling limits. (c)-(e) Exemplary multi-Lorentzian fits for three indicated interactions strengths.

with the residue Z , the energy E and the lifetime τ as fitting parameters. In Fig. S3, we show the results for E and τ across a range of interactions strengths J/t , with exemplary multi-Lorentzian fits shown in Figs. S3(c)-S3(e).

-
- [1] G. F. Reiter, Phys. Rev. B **49**, 1536 (1994).
 - [2] K. K. Nielsen, M. A. Bastarrachea-Magnani, T. Pohl, and G. M. Bruun, Phys. Rev. B **104**, 155136 (2021).
 - [3] S. Schmitt-Rink, C. M. Varma, and A. E. Ruckenstein, Phys. Rev. Lett. **60**, 2793 (1988).
 - [4] C. L. Kane, P. A. Lee, and N. Read, Phys. Rev. B **39**, 6880 (1989).
 - [5] G. Martinez and P. Horsch, Phys. Rev. B **44**, 317 (1991).
 - [6] Z. Liu and E. Manousakis, Phys. Rev. B **44**, 2414 (1991).
 - [7] A. Ramšak and P. Horsch, Phys. Rev. B **57**, 4308 (1998).